



# OPEN Sustainable mobility with renewable hydrogen: a framework for refueling station design and optimisation using liquid organic hydrogen carriers (LOHCs)

Mradul Dhakar<sup>1,4</sup>, Mengyu Wang<sup>2</sup>, Ahmad Rafiee<sup>3</sup>, Yun Liu<sup>4</sup>, Igor Skryabin<sup>1</sup> & Kaveh Khalilpour<sup>2</sup>✉

Hydrogen fuel cell vehicles (HFCVs) are key to long-term decarbonisation strategies. However, their widespread adoption hinges on the availability of hydrogen refuelling stations and the ability to lower the at-the-pump price of hydrogen. This study conducts a detailed techno-economic analysis of a hydrogen refuelling station that features on-site production via water electrolysis, storage, and dispensing infrastructure. Using a least-cost optimisation model, the total annualised cost (TAC) is minimised while meeting mass and heat flow constraints. The system is fully electrified, relying entirely on electricity for all processes, including heating for the liquid organic hydrogen carriers (LOHC) system. The analysis explores three scenarios: variations in electricity sources, differences in renewable energy pricing, and the integration of various LOHCs. Results demonstrate that a grid-connected hydrogen refuelling system employing LOHCs provides a competitive production cost and a higher capacity factor. Intermittency impacts system design, increasing capital costs to ensure optimal sizing. Among LOHCs, N-ethylcarbazole is identified as particularly effective, offering resilience and efficiency under variable conditions. Applying this model in Canberra, Australia, the system achieves hydrogen dispensation costs of under A\$8/kg<sub>H<sub>2</sub></sub>, showcasing its potential for scalable, cost-effective hydrogen refuelling infrastructure.

**Keywords** Sustainable mobility, Hydrogen refuelling station, Liquid organic hydrogen carrier (LOHC), Green hydrogen production, Techno-economic analysis

Greenhouse gases emitted from human activities have increased significantly over the past decades, leading to climate change. Transport contributes to approximately one-fifth of global carbon emissions. Around 75% of these emissions are generated by road transport<sup>1</sup>. Among road vehicles, passenger vehicles account for the largest share at 45.1%. In 2021, the global CO<sub>2</sub> emissions produced by transport experienced a rebound and returned to their historical growth trend. With the Paris Agreement, many countries are committed to reducing carbon emissions. To meet the net-zero emission target by 2030, hydrogen gas has the potential to be used as an energy carrier in transport, power generation and a range of manufacturing industries.

Hydrogen fuel cell vehicles (HFCVs) are becoming commercially attractive in long-term decarbonisation strategies. They are fuel cell vehicles that use pressurised hydrogen as an energy carrier. Currently, there are only a few commercial Hydrogen Fuel Cell Electric Vehicle (HFCEVs) available in the market, such as Toyota Mirai and Hyundai Nexo. Similar to fossil fuel vehicles, the growth of HFCEVs requires a network of hydrogen refuelling stations (HRS) to be well-established across the country. As of 2023, about 921 HRS were in operation worldwide, of which 197 were located in China and 724 in the rest of the world<sup>2</sup>. To increase the adoption of HFCEVs, it is necessary to accelerate the development of hydrogen infrastructure and lower the at-the-pump price of hydrogen fuel.

<sup>1</sup>ANU Institute for Climate, Energy & Disaster Solutions, Australian National University, Canberra, Australia.

<sup>2</sup>Faculty of Engineering and IT, University of Technology Sydney, Sydney, Australia. <sup>3</sup>Department of Mechanical and Biomedical Engineering, University of Galway, Galway, Ireland. <sup>4</sup>Research School of Chemistry, Australian National University, Canberra, Australia. ✉email: kaveh.khalilpour@uts.edu.au

Hydrogen production is the largest cost contributor to the hydrogen prices offered to customers<sup>3</sup>. Hydrogen can be produced through various methods. To date, almost 95% of hydrogen is produced from natural gas at centralised facilities and delivered by trucks or pipelines. Steam methane reforming (SMR) has been the most widespread method used for large-scale hydrogen production<sup>4</sup>. Hydrogen produced through this pathway, although relatively low-cost, faces multiple limitations, including but not limited to (1) reliance on finite fossil fuels, (2) reliance on carbon capture technologies, and (3) being distant from the end-user. The emergence of distributed generation and storage technologies has increased interest in the so-called “green hydrogen”, which is (1) reliant on practically an infinite source of energy (e.g., sun/wind), (2) no GHG gas emissions, and (3) the production facility can be located at demand-side, eliminating the need for hydrogen transportation. However, renewable resources such as solar and wind have intermittent and non-dispatchable issues, which may have a significant impact on the security and reliability of hydrogen supply. Further, the hydrogen production rate is limited by the capacity of the electrical grid at the location HRS location. This becomes more critical for cases such as refuelling stations with further uncertainty in the refuelling pattern of customers. Therefore, the integration of storage facilities is essential to mitigate the imbalance between hydrogen supply and demand, ensuring a consistent and reliable energy flow. This paper aims to provide a solution for the design and operation of such a dynamic HRS. To do that, we first need to choose hydrogen storage technology. For this study, we have selected liquid organic hydrogen carriers for the reasons discussed next.

### Liquid organic hydrogen carriers (LOHC)

Several existing methods and technologies are available for storing hydrogen<sup>5</sup>. These include physical-based (i.e. compressed gas at 350 or 700 bar, liquid hydrogen storage, and cryogenic-compressed gas storage) or material-based (i.e. physisorption and chemisorption) methods. The use of liquid organic hydrogen carrier (LOHC) as a chemisorption technology has demonstrated potential for hydrogen storage and transportation. Figure 1 shows a simplified schematic of this process. The storage process, or hydrogenation, involves a catalytic reaction between hydrogen and a LOHC chemical. The product is then stored until use when a reverse reaction, or dehydrogenation, is carried out to recover hydrogen (to be used) and the LOHC (to be recycled). One key advantage of this process is that the LOHC can be stored and distributed as a liquid at ambient temperature and pressure at both loaded and unloaded conditions.

The selection of LOHC candidates is typically based on their thermodynamic properties, economy, safety, and environmental impacts. Various LOHCs used for hydrogen storage and transportation have been compared in several studies<sup>6–8</sup>. The most widely developed LOHCs are methylcyclohexane (MCH), toluene (TOL), dibenzyltoluene (DBT), and N-ethylcarbazole (NEC), which are cheap and easily accessible. Reference<sup>8</sup> Crabtree assessed a group of potential LOHC materials used as hydrogen carriers, considering their simplicity, safety, scalability, heat management, and economic viability<sup>9</sup>. Liquid heterocyclic aromatic hydrocarbons were concluded as the most feasible carriers thermodynamically. Müller et al.<sup>10</sup> presented a study on thermodynamic properties of LOHC materials and suggested that nitrogen-containing aromatic compounds were more suitable for this purpose. The enthalpy of these organic compounds should be greater than 40 kJ/mol of H<sub>2</sub>. Their current research on LOHCs found that both dibenzyltoluene and benzyltoluene are promising materials used as hydrogen carriers due to their thermophysical and thermochemical properties<sup>11</sup>. Brückner et al.<sup>12</sup> carried out an experimental study on the thermodynamic suitability of heat-transfer fluids used as LOHC systems. Benzyltoluene and dibenzyltoluene were excellent storage materials for use in the excessive production of hydrogen because of their good performance in hydrogenation and dehydrogenation reactions. First, both compounds were characterised by high hydrogen storage capacities without solidification (−30 °C or below), while N-ethylcarbazole was a solid at ambient conditions. Second, they had lower vapour pressure and less harmful toxicological effects than toluene/methylcyclohexane and naphthalene/decalin.

In 2018, Chiyoda Corporation in Japan built a pilot plant using SPERA technology for large-scale hydrogenation and dehydrogenation. Methylcyclohexane and toluene were identified as the most promising carriers<sup>13</sup>. Niermann et al.<sup>14</sup> found that methanol was the most cost-effective carrier, followed by dibenzyltoluene and toluene. Although LOHCs have been considered for storage and transportation of hydrogen in various applications<sup>15–19</sup>, their applications in HRS have not been widely investigated.

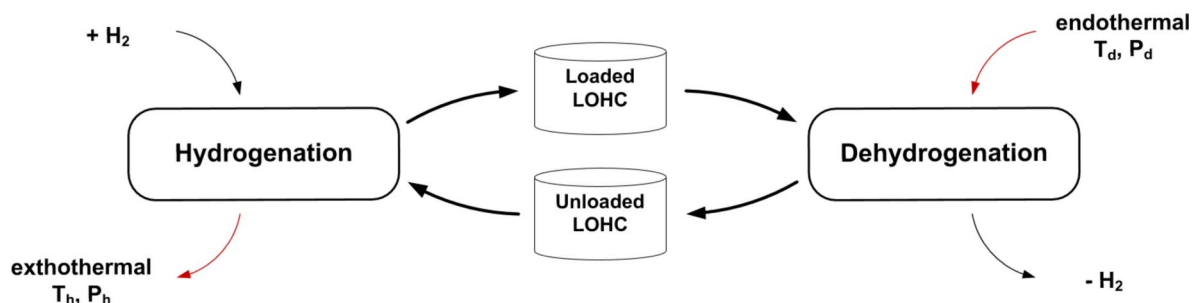


**Fig. 1.** A simplified schematic of the LOHC process.

## Hydrogen refuelling station design with LOHCs

Techno-economic optimisation of HRS is crucial for improving energy efficiency and determining the hydrogen production cost (HPC). It is noteworthy that HPC indicates the same value as the widely used term LCOH (levelised cost of hydrogen). However, this paper uses the former to avoid confusion between the terms LCOH and LOHC. As summarised in Table 1, several studies have conducted techno-economic assessments considering onsite hydrogen production powered by grid electricity (generated from fossil fuel, hydropower, and biomass) and renewable energy, while the selected LOHC systems for hydrogen storage have not been revealed. The calculated HPC values range from \$3.73/kg to \$63.8/kg, depending on process configurations, renewable energy costs, and assumptions for key input parameters. For example<sup>20</sup> reported a low HPC value of \$3.73/kg, excluding the cost of compression, storage, and dispensing units. Although design optimisation of HRS has been carried out by Ref.<sup>21–25</sup>, it has not been done for the entire hydrogen supply chain. Therefore, the development of a comprehensive framework for evaluating the cost and performance of all system components would provide a fair comparison of HPC values across the literature.

This study is motivated by a demonstration case where the Australia Research Council has provided funding support to investigate the integration of hydrogen storage via LOHCs into a commercialized hydrogen refuel station in Canberra, Australia. In its planning phase, this study investigates the technical and economic feasibility of a hydrogen refuelling station using solar power as the main source of electrical power and LOHCs for hydrogen storage. The outline of the article is as follows: Section "System components of the HRS model" looks at a hydrogen refuelling station (HRS) with onsite hydrogen production, hydrogen storage, heat management, and dispensing units. Section "Modelling approach" covers the process flow diagram of the HRS, the modelling tools used in the paper, the model inputs, the formulation of the optimisation model, and the techno-economic analysis of HRS. In Section "Scenario analysis", the scenario analysis is presented to pinpoint the impacts of the variations in power supply sources, the type of LOHC materials, and changes in renewable energy prices on the performance and cost of the HRS. Section "Conclusions" concludes our study.

## System components of the HRS model

Hydrogen can be imported to hydrogen refuelling stations (HRS) as with conventional petrol, diesel, or CNG fuel stations, or can be generated onsite through electrolyser technologies. This study focuses on the HRS with onsite hydrogen production, hydrogen storage, heat management, and dispensing units, as shown in Fig. 2.

## Hydrogen production

Hydrogen is produced via water electrolysis in a PEM electrolyser powered by renewable electricity from either an onsite solar PV system or the grid. When water passes through the electrolyser, it is dissociated into positively charged hydrogen ions and negatively charged oxygen ions by electric current. Hydrogen and oxygen are formed at the cathode and anode sides of the electrolysis cell, respectively. This process converts electrical energy into chemical energy stored in hydrogen.

There are two pathways for keeping hydrogen supply and demand in balance at the HRS. One pathway is directly delivering hydrogen to the dispensing unit for instantaneous demand. When the amount of hydrogen produced exceeds its demand, excess hydrogen will be stored in a hydrogen carrier through the hydrogenation process and used later.

## Hydrogen storage

The hydrogen storage unit is designed to store the excess hydrogen from the electrolyser. Two reversible reactions are involved, which are hydrogenation and dehydrogenation. When hydrogen reacts with a hydrogen-

Location	Power sources	Connection type	H <sub>2</sub> production (kg/day)	HPC (\$/kg H <sub>2</sub> )	H <sub>2</sub> storage technology	Optimisation	Reference
Sweden	Wind	Standalone	1600	5.18–9.62	Pressurised tank	Y	25
California	Solar, wind	Standalone	–	9.14 for solar, 6.71 for wind	Pressurised tank	–	26
Saudi Arabia	Solar, wind, hybrid wind-solar	Standalone		39.5–63.8	Battery bank storage system, hydrogen tank		27
Turkey	Hybrid system: wind-solar-battery, wind-battery	Standalone	125	8.92 for hybrid wind-PV-battery, 11.08 for wind-battery	Buffer storage tank	Y	28
Brazil	Solar	Standalone	20–185	8.96–13.55	Pressurised tank	–	29
Norway	Hydropower	Standalone	33	8.45–10.08 with 50% public support, 14.35–15.98 with no public support	High-pressure tank	–	30
South Africa	Wind	Standalone	125	6.034–8.97	Pressurised tank	Y	21
China	Solar, wind, grid	Standalone and grid-connected	500	14.61–40.31	Pressurised tank	Y	23
Ghana	Solar, wind, biomass	Standalone	152	9.09 for hybrid biomass-solar	Pressurised tank	Y	22
Tunis	Solar	Standalone	150	3.73*	–	–	20

**Table 1.** Related studies of standalone/grid-connected hydrogen refuelling stations. \*The compression, storage, and dispensing unit costs were not included.

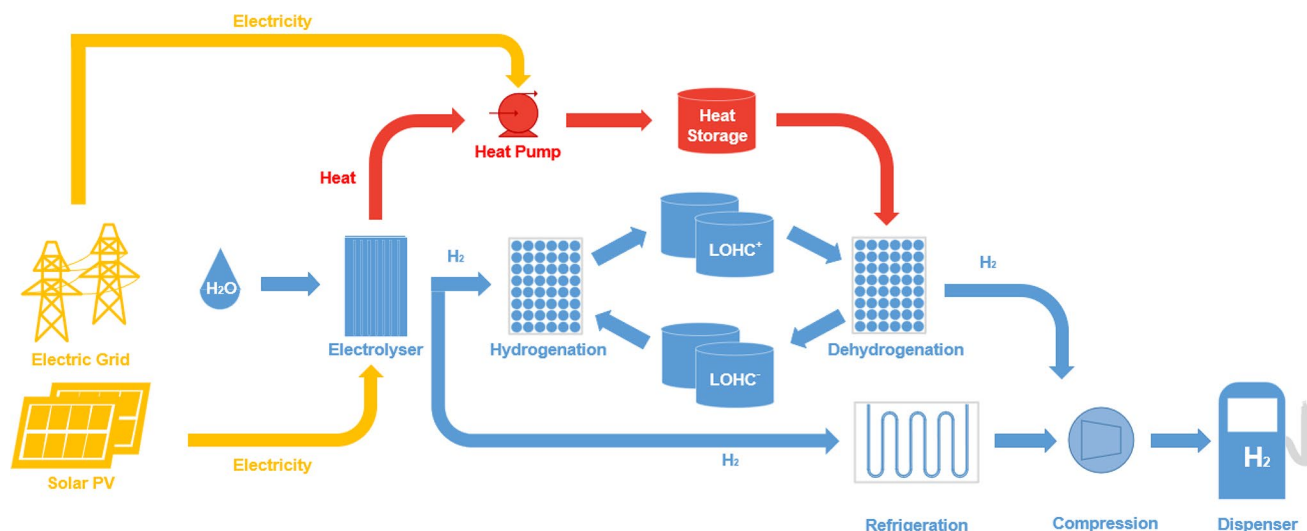


**Fig. 2.** Schematic diagram of a hydrogen refuelling station using liquid organic hydrogen carriers.

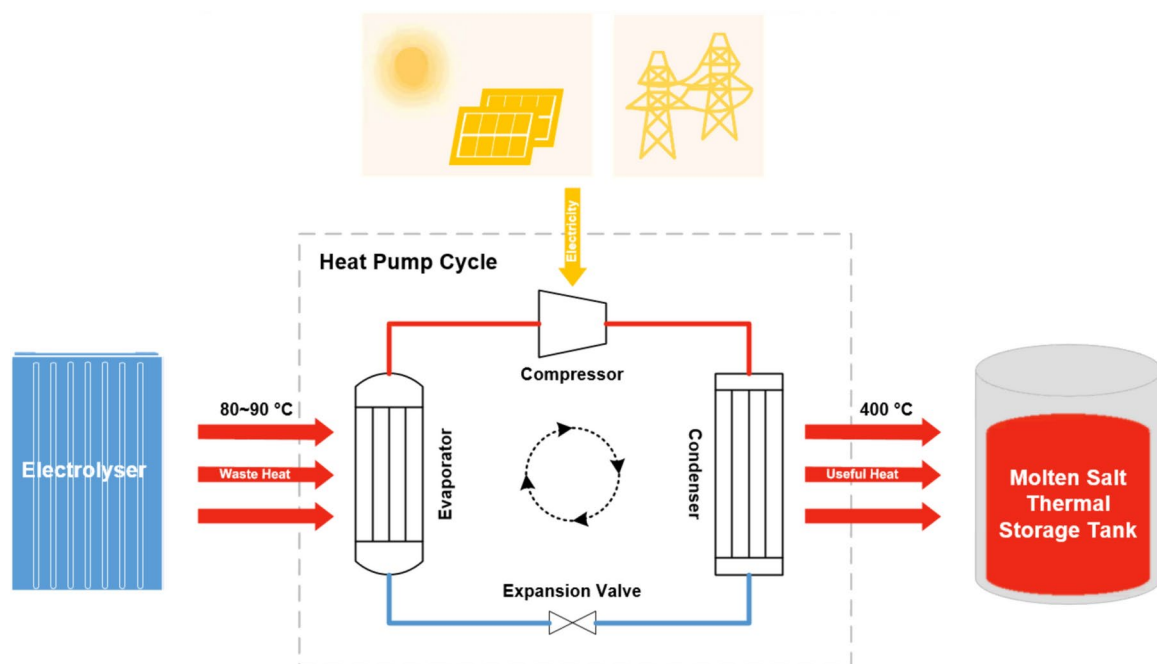


**Fig. 3.** Heat pump cycle with a molten salt thermal energy storage tank.

lean carrier in the hydrogenation reactor at a temperature of 150 °C and a pressure of 30 bar, a hydrogen-rich carrier is formed as a product and stored in a hydrogenation storage tank. When the stored hydrogen is required, the hydrogen-rich carrier is pumped to the dehydrogenation reactor at a temperature of 310 °C and a pressure of 1 bar. It is then dissociated into a hydrogen-lean carrier. Hydrogen is sent to the dispensing unit as a fuel product and hydrogen-lean carrier is stored in the dehydrogenation storage tank. In this study, dibenzyltoluene (DBT) is chosen as a hydrogen-lean carrier, and perhydro-dibenzyltoluene (PDBT) as a hydrogen-rich carrier for the base case analysis.

### Heat management

In the heat management unit, the waste heat energy released from the electrolyser is captured by a heat pump at a low temperature of 75~85 °C and then retrieved into a molten salt thermal energy storage tank at a high temperature of around 400 °C. The commercial liquid media used in the thermal energy storage tank is called solar salt, which is a mixture of 60 wt.% NaNO<sub>3</sub> and 40 wt.% KNO<sub>3</sub>. The thermal heat is transferred from the thermal energy storage tank through heat exchangers to the dehydrogenation reactor, when it is needed. Figure 3



shows a simplified process diagram of the heat pump cycle integrated with a molten salt thermal energy storage tank.

Due to the high-temperature difference between the waste heat source and thermal energy storage tank, cascade heat pumps are an ideal solution to efficiently provide heat to the system at high temperatures. These heat pumps have been developed for industrial applications, particularly for concentrated solar thermal power (CSTP) plants. However, they are highly complex and high-cost equipment. For simplicity, a single-stage heat pump is assumed to transfer low-temperature heat to the thermal energy storage tank operating at high temperatures in this study.

### Hydrogen dispensation

The hydrogen dispensing unit is designed to refuel the vehicles with hydrogen fuel. It comprises refrigeration, compression, and dispensing equipment<sup>31</sup>. The hydrogen outlet pressure from the PEM electrolyser is 30 bar, while the dehydrogenation reactor has a discharge pressure of 1 bar. Prior to blending the two hydrogen streams, the outlet pressure from the electrolyser is reduced to 1 bar through a throttle valve. A blend of hydrogen is then precooled to -40 °C with a refrigerator and compressed to the desired pressure of 700 bar using a reciprocating compressor before dispensing. This process helps prevent the vehicle's on-board storage tank from overheating and overpressuring.

### Modelling approach

The optimal scheduling model was developed to minimise the total annualised cost of an HRS considering the hydrogen supply chain and LOHC technology. The use of a least-cost optimisation model for operational scheduling in hydrogen refuelling stations is justified by its ability to identify the most cost-effective strategies for producing, storing, and dispensing hydrogen while balancing supply with fluctuating demand. By integrating variables such as energy prices, production rates, storage capacity, and refuelling patterns, the model minimises operational expenses and ensures an efficient use of resources. This approach is critical in achieving low-cost hydrogen, as it systematically reduces inefficiencies, optimises the timing of energy-intensive processes to align with lower electricity tariffs, and ensures reliable service delivery. Additionally, it provides a robust framework to adapt to dynamic market conditions and regulatory requirements, further supporting hydrogen infrastructure's economic viability and scalability. Figure 4 provides an overview of the methodological framework for this study covering process inputs and constraints, scenario analysis, optimisation, and a detailed technical and economic analysis. Scenario analyses were undertaken to understand how the changes in electricity supply sources, fluctuations in renewable energy prices, and the selection of LOHCs can affect the HPC and equipment sizing. By examining these scenarios, this study could identify the key factors that may impact the commercial viability of the HRS using various LOHCs.

### Process model

The proposed process model considers an HRS with the entire hydrogen supply chain, including hydrogen demand forecast, hydrogen production, hydrogen storage, heat management, and dispensing units as illustrated in Fig. 5. As the hydrogen dispensation systems were the same for all scenarios, they were not considered as part of the analytical framework for technical feasibility and cost analysis.

### Modelling tools

Julia is an open-source programming language that was used in this study for the linear programming (LP)-based optimisation problem for the HRS. The Gurobi optimiser was used to build a cost optimisation model within the Julia environment. The optimisation was performed in hourly intervals to account for the reaction time of the hydrogenation and dehydrogenation processes.

System Advisor Model (SAM) is a free modelling software developed by the National Renewable Energy Laboratory (NREL) for performance and cost analysis in the renewable energy industry<sup>32</sup>. The SAM 2020 model has been used with Acton, Canberra, Australia, as the location used. The PV module, inverter technical specifications, and the system design details are provided in the Supplementary file (Section S1).

### Model inputs

Four input variables are selected for the performance and cost evaluation of the HRS, including the solar PV generation profile, grid electricity price profile, estimated capital cost (CAPEX) and operating cost (OPEX), and hydrogen demand profile. These variables were predicted using time-series modelling data. One of the input variables is solar power, predicted through the time series modelling of the onsite solar PV system using the System Advisor Model, which is used for hydrogen production via water electrolysis. The solar energy yield is dependent on the sunlight hours per day and, therefore, varies throughout the year. Figure 6 shows the hourly average electricity generated from a 1000 kW solar PV plant located in Acton, Canberra between 1st January and 31 December. The peak solar irradiation levels occur between November and March, while the lower solar irradiation levels are observed from May to August.

Grid electricity price profile is the second input variable of the proposed HRS model. It was obtained from Regional Reference Prices (RRP) for New South Wales (NSW) across the National Electricity Market (NEM) in 2020. The electricity price is typically settled in a 30-min trading interval for each NEM region. In this study, the electricity price is calculated on an hourly basis, which is the average of the two consecutive trading interval prices.

The hydrogen demand profile is an important input variable for the optimisation of the HRS. In this study, the hydrogen refuelling behaviour in Canberra was derived based on the modified Chevron profile from the Hydrogen Refuelling Station Analysis Model (HRSAM) and the hydrogen demand profile from the California

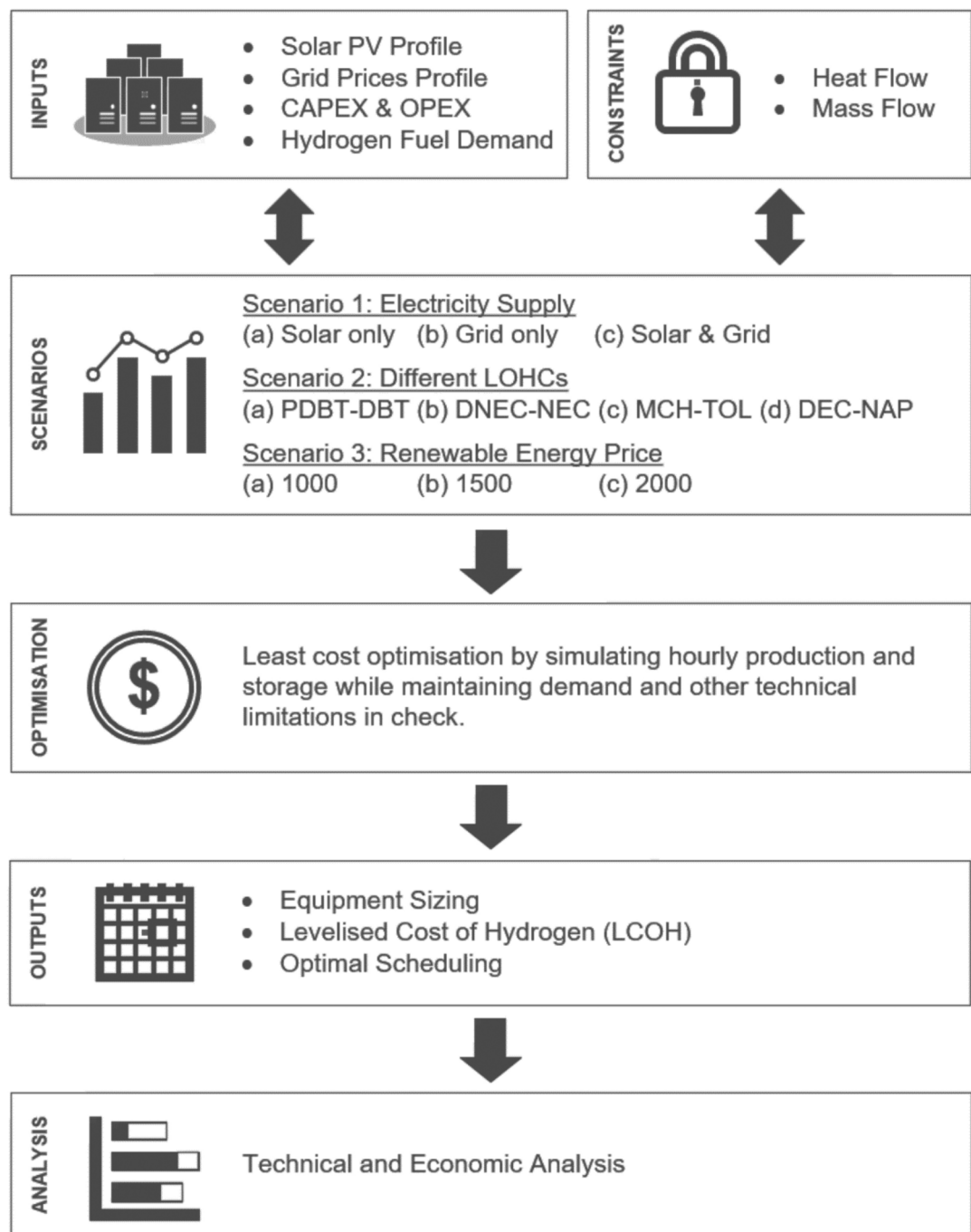


**Fig. 4.** An overview of the methodological framework.

Energy Commission (CEC) paper. The CEC profile was chosen because California's geography and population density are similar to Australia's east coast. By 2022, there were approximately 43 hydrogen refuelling stations and 6826 registered HFCVs in California<sup>33</sup>.

As presented in Fig. 7, the total hydrogen demand at the HRS is 500 kg per day. The peak hydrogen demand reaches 39.5 kg/hour at 5:00 pm every day, which accounts for approximately 7.9% of the total daily hydrogen demand. The lowest hydrogen demand is only 2.5 kg/hour at 4:00 am.

CAPEX and OPEX are the key input variables for economic analysis of the HRS. The procurement cost for equipment is an essential factor that can significantly affect the overall cost estimations. However, the costs associated with the grid connection system are not considered, since the grid electricity is purchased from the existing renewable power plants. The model assumptions are provided as Supplementary data (Section S2).

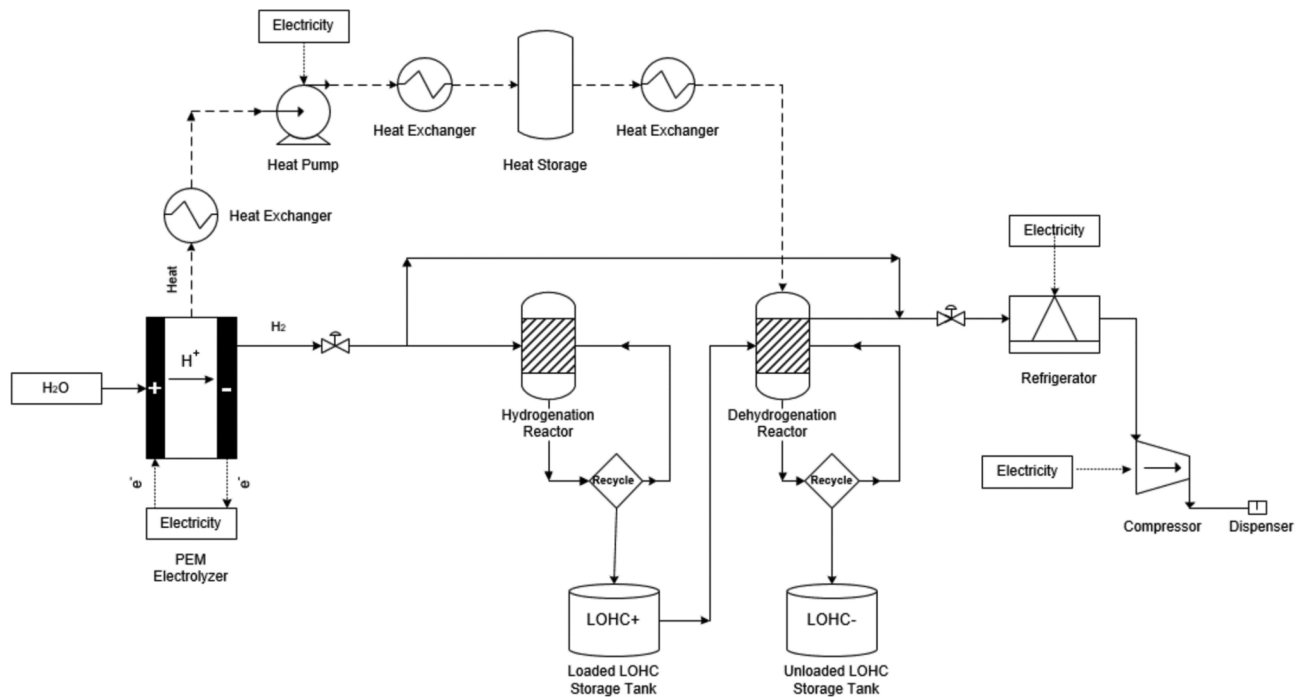


Fig. 5. Process flow diagram of a hydrogen refuelling station using LOHC technology.

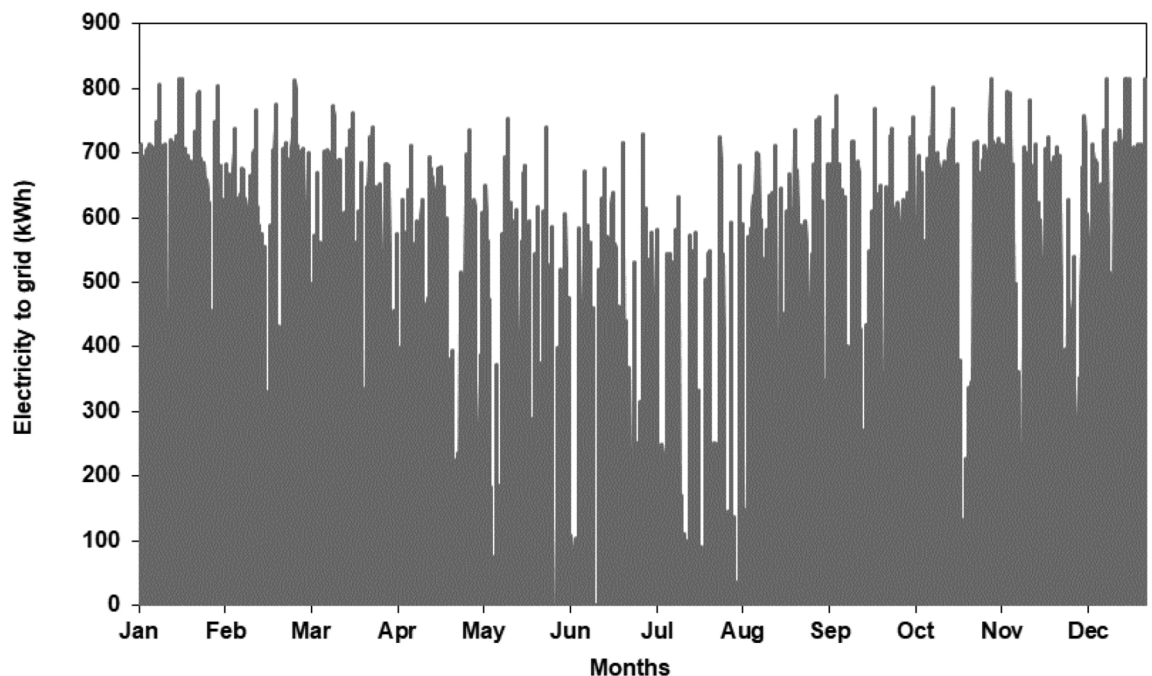


Fig. 6. Hourly average solar electricity generated at Acton, Canberra.

### Mathematical optimisation formulation

**Objective function:** The objective function of the cost optimisation model is to minimise the total annualised cost (*TAC*) of an HRS with a hydrogen supply chain while meeting the daily supply and demand of hydrogen fuel, as shown in Eq. (1):

$$\min.TAC = CAPEX + OPEX_{\text{fixed}} + OPEX_{\text{variable}} \quad \min.TAC = CAPEX + OPEX_{\text{fixed}} + OPEX_{\text{variable}} \quad (1)$$

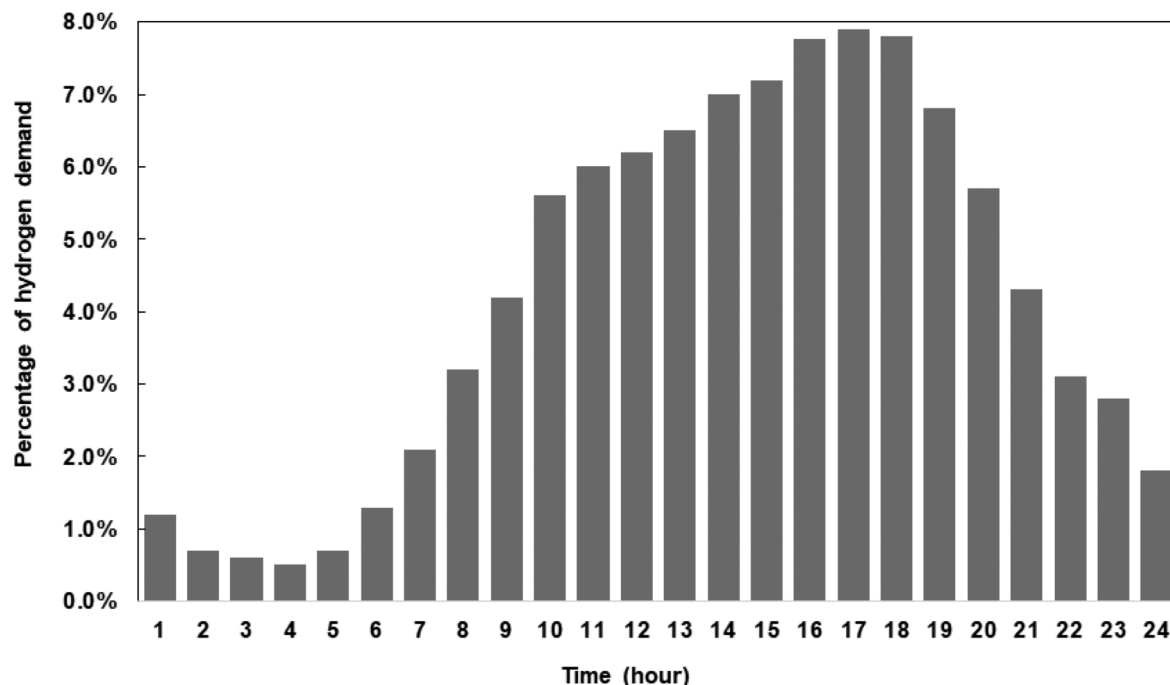


Fig. 7. Hourly hydrogen demand at the hydrogen refuelling station.

Constraints: There are four sets of constraints (Table 2); (1) Hydrogen mass flow conservation, (2) Desing capacity, (3) Hydrogen storage, and (4) Heat management.

### Techno-economic analysis of HRS

This section provides a theoretical understanding of how an HRS using different LOHC pairs for hydrogen storage could work and its economic performance. The proposed HRS consists of four main units: hydrogen production, storage, heat management, and dispensing. However, the hydrogen dispensing unit is excluded from the techno-economic model since it is already a commercialised and highly matured technology that has been extensively studied in academic literature.

#### Technical model

**Hydrogen production** PEM electrolyser releases excessive heat during electrochemical reaction. The actual waste heat ( $Q_c$ ) from the electrolysis process at a given time can be expressed as:

$$Q_c = (E_{i,j} - L) \cdot \eta_{\text{electrolyser}} \cdot y_{i,j} \cdot \varepsilon \quad (18)$$

where,  $E_{i,j}$  is specific electrical consumption of the electrolyser ( $\text{kWh/kg}_{\text{H}_2}$ ),  $L$  is a specific lower heating value of hydrogen ( $33.33 \text{ kWh/kg}_{\text{H}_2}$ ),  $\eta_{\text{electrolyser}}$  is the heat loss coefficient of a PEM electrolyser (%),  $y_{i,j}$  is hydrogen production rate at the  $i$ th hour of the  $j$ th day throughout the year ( $i = 1, 2, 3, \dots, 24; j = 1, 2, 3, \dots, 365$ ), and  $\varepsilon$  is the effectiveness of the heat exchangers (0.8).

**Hydrogen storage** The hydrogen storage tank is used to supply hydrogen gas when the hourly hydrogen demand at the HRS is higher than the daily average. Two processes are involved in the hydrogen storage unit: hydrogenation and dehydrogenation. Table 3 summarises the selected LOHCs' reaction mechanisms, their chemical structures, and physical–chemical properties. The performance of the hydrogenation and dehydrogenation reactors is related to mass conversion and yield of hydrogen in a time series. According to the law of conversion of mass, the mass conversion of hydrogen is defined in Eqs. (19) and (20).

For loaded LOHC tank,

$$m_{1,i+1,j} = m_{1,i,j} + (u_{i,j} - v_{i,j}) \cdot x_1 \quad (19)$$

For unloaded LOHC tank,

$$m_{2,i+1,j} = m_{2,i,j} + (u_{i,j} - v_{i,j}) \cdot x_2 \quad (20)$$

where,  $m_{1,i+1,j}$  is the mass of loaded LOHC in the loaded LOHC tank (kg),  $m_{2,i+1,j}$  is the mass of unloaded LOHC in the unloaded LOHC tank (kg),  $u_{i,j}$  and  $v_{i,j}$  are hydrogenation rate and dehydrogenation rate, respectively,  $x_1$  and  $x_2$  are the conversion, which is the stoichiometric ratios of loaded or unloaded LOHC to hydrogen, respectively.

Constraint type		
Hydrogen mass flow conservation	$y_{i,j} - u_{i,j} + v_{i,j} = x_{i,j}$ Where, $y_{i,j}$ , $u_{i,j}$ , $v_{i,j}$ , and $x_{i,j}$ represent hydrogen production rate, hydrogenation rate, dehydrogenation rate, and hydrogen demand rate at the $i^{th}$ hour of the $j^{th}$ day throughout the year ( $i = 1, 2, 3, \dots, 24; j = 1, 2, 3, \dots, 365$ ) respectively	(2)
Desing capacity	$0 \leq y_{i,j} \leq y_1$ Where, $y_1$ is the design capacity of the electrolyser	(3)
	$0 \leq u_{i,j} \leq u_1$ Where, $u_1$ is the design capacity of the hydrogenation reactor	(4)
	$0 \leq v_{i,j} \leq v_1$ Where, $v_1$ is the design capacity of the dehydrogenation reactor	(5)
	$648 \leq m_{1,i,j} \leq m_1$ Where, $m_1$ is the design capacity of the hydrogenation storage tank, and $m_{1,i,j}$ is the mass of loaded LOHC in the loaded LOHC tank	(6)
	$648 \leq m_{2,i,j} \leq m_2$ Where, $m_2$ is the design capacity of the dehydrogenation storage tank, and $m_{2,i,j}$ is the mass of unloaded LOHC in the unloaded LOHC tank	(7)
	$0 \leq h_1 \leq 100$ Where, $h_1$ is heat pump design capacity	(8)
	$540 \leq H_1$ Where, $H_1$ is the heat exchanger design capacity	(9)
	$0 \leq E_{i,j} \leq E_1$ Where, $E_1$ is the maximum power capacity of the electrolyser, and $E_{i,j}$ is the specific energy consumption of the electrolyser	(10)
Hydrogen storage	The total hydrogenation rate is greater than the total dehydrogenation rate $\sum u \geq \sum v \geq 0$	(11)
	The total hydrogen demand is greater than the total dehydrogenation rate $\sum x \geq \sum v \geq 0$	(12)
	The difference between hydrogenation rate and dehydrogenation rate should exceed the design capacity of the dehydrogenation reactor $u - v \geq -v_1$	(13)
	The difference between hydrogenation rate and dehydrogenation rate should be less than the design capacity of the hydrogenation reactor $u - v \leq u_1$	(14)
Heat management	The energy flow rate of the heat pump is measured in kWh/50 kg <sub>H2</sub> for scaling purposes $y_{i,j} + h = \frac{E_{i,j}}{50}$	(15)
	The heat pump efficiency ( $h$ ) is: $h \leq (\frac{12}{50}) \cdot y$	(16)
	The thermal heat is transferred from a molten salt thermal energy storage tank through heat exchangers into the dehydrogenation reactor. It is assumed that the energy efficiency ( $\eta$ ) is 99% in this study $H_{i+1,j} = [H_{i,j} + 101 \cdot h_{i,j} - 12 \cdot v_{i,j}] \cdot \eta$	(17)

**Table 2.** Constraints of the model.

Space–time yield (STY) is the amount of hydrogen produced in moles per volume of reactor and unit of time for a given conversion rate. The sizing of the reactors can be compared through the *STY* formulated in Eq. (21).

$$STY = \frac{n_A x_A}{v_R t_R} \quad (21)$$

where,  $n_A$  is the amount of hydrogen yield (mol),  $x_A$  is the conversion, which is the stoichiometric ratio of LOHC to hydrogen,  $v_R$  is the volume of hydrogenation or dehydrogenation reactor, and  $t_R$  is the reaction time, which is assumed to be 1 h for each LOHC.

**Heat management** The heat management unit is a reverse-cycle heat pump integrated with three heat exchangers and a thermal energy storage (TES) tank. The heat pump captures waste heat from the electrolyser ( $Q_c$ ) at a low temperature  $T_c$  as the heat inlet and utilises work input from an electricity source to raise the waste heat to a high temperature  $T_h$ . According to the first law of thermodynamics, the heat releases ( $Q_h$ ) from the heat pump is estimated using Eq. (22).

$$Q_h = Q_c + W \quad (22)$$

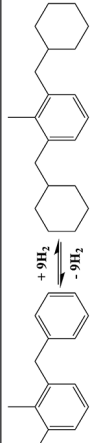
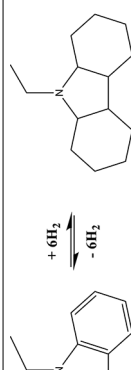

The coefficient of performance (COP) represents the efficiency of the heat pump.

$$COP = \frac{Q_h}{W} \quad (23)$$

Substituting (22) to (23),

$$COP - 1 = \frac{Q_c}{W} = s \quad (24)$$



LOHC	Hydrogen storage capacity (wt.%)	Enthalpy (kWh/kg <sub>H<sub>2</sub></sub> )	Formula		Molecular weight (g/mol)		Hydrogenation			Dehydrogenation		
			Loaded LOHC	Unloaded LOHC	Loaded LOHC	Unloaded LOHC	T <sub>h</sub> (°C)	P <sub>h</sub> (bar)	STY (mol <sub>H<sub>2</sub></sub> /L·h)	T <sub>d</sub> (°C)	P <sub>d</sub> (bar)	STY (mol <sub>H<sub>2</sub></sub> /L·h)
 <p>Dibenzyltoluene (DBT)</p> <p>Perhydro-Dibenzyltoluene (PDBT)</p>	6.21	9.78	C <sub>21</sub> H <sub>38</sub>	C <sub>21</sub> H <sub>20</sub>	290	272	150	50	278.80	310	1	13.75
	5.80	7.60	C <sub>14</sub> H <sub>25</sub> N	C <sub>14</sub> H <sub>13</sub> N	207	195	160	50	218.20	270	1	30.75
 <p>N-ethylcarbazole (NEC)</p> <p>Dodecahydro-N-ethylcarbazole (DNEC)</p>	6.52	9.50	C <sub>7</sub> H <sub>14</sub>	C <sub>7</sub> H <sub>8</sub>	92	86	200	50	466.20	320	1	22.40
 <p>Toluene (TOL)</p> <p>Methylcyclohexane (MCH)</p>	6.76	9.20	C <sub>10</sub> H <sub>18</sub>	C <sub>10</sub> H <sub>8</sub>	148	138	200	69	388.20	280	1	81.55

**Table 3.** Reaction mechanism of the selected LOHCs and their chemical structure and physical–chemical properties.

where,  $s$  is a ratio of waste heat to work input of the heat.

Reverse Carnot equation for heat pump

$$\frac{Q_c}{W} = s \cdot u = \left( \frac{T_c}{T_h} - T_c \right) u \quad (25)$$

A molten salt thermal energy storage tank uses a mixture of  $\text{NaNO}_3$  and  $\text{KNO}_3$  as the heat transfer fluid to store the heat from the heat pump for later use in the dehydrogenation reactor. The heat conversion ( $\text{TES}_{i+1,j}$ ) in the thermal energy storage tank is given by

$$\text{TES}_{i+1,j} = \left( \frac{(\text{TES}_{i,j} + (E - L) \eta_{\text{electrolyser}} y_{i,j} \varepsilon^2 (1 + s_1 u))}{s_1 u} - v_{i,j} \frac{H}{\varepsilon \mu_2} \right) \cdot l \quad (26)$$

where  $v_{i,j}$  is dehydrogenation rate,  $s_1$  is the ratio of heat source and work for the electrolyser,  $H$  is the enthalpy of dehydrogenation ( $\text{kWh/kg}_{\text{H}_2}$ ), and  $\mu_2$  is degree of dehydrogenation.

**Capacity factor** The capacity factor (CF) is the ratio of the actual output produced by a generating unit to its total installed capacity over a time period of  $t$ . It mainly depends on the size of the equipment and is expressed by

$$\text{CF} = \frac{E_{\text{annual}}}{C_t} \quad (27)$$

where,  $C_t$  is the total installed capacity of the equipment, and  $E_{\text{annual}}$  is the total actual output for a period of time.

#### Economic model

The economic model is proposed to evaluate the cost performance of the HRS, which is determined by the main units' capital, operation and maintenance costs.

**Hydrogen production cost** HPC Is used to evaluate the economic feasibility of the HRS during its designated lifetime. It is calculated based on the cost input variables and assumptions summarised in Sect. 3.3.2, but may vary with the use of different energy supply sources. The HPC for the HRS with a hydrogen production capacity of  $500 \text{ kg}_{\text{H}_2}/\text{day}$  is calculated by

$$\text{HPC} = \frac{C_{\text{annual}}}{m_{\text{H}_2}} \quad (28)$$

where  $C_{\text{annual}}$  is the total annualised cost ( $\text{\$/year}$ ),  $m_{\text{H}_2}$  is the total hydrogen production per year ( $\text{kg}_{\text{H}_2}/\text{year}$ ).

**Total annualised cost** Total annualised cost ( $C_{\text{annual}}$ ) is a sum of the total capital expenditure ( $C_{\text{capital}}$ ), and operation and maintenance (O&M) costs ( $C_{\text{operating}}$ ) of each system component per year, which is represented as:

$$C_{\text{annual}} = C_{\text{capital}} + C_{\text{operating, fixed}} + C_{\text{operating, variable}} \quad (29)$$

where  $C_{\text{capital}}$  is total capital expenditure ( $\text{\$/year}$ ),  $C_{\text{operating, fixed}}$  is total fixed operating expenditure ( $\text{\$/year}$ ), and  $C_{\text{operating, variable}}$  is total variable operating expenditure ( $\text{\$/year}$ ).

The capital and operating costs are the largest components of the total annualised cost. In this study, the total annualised cost is calculated by multiplying the total capital investment ( $C_{\text{TCI}}$ ) by the annuity factor  $\frac{(1+r)^n}{(1+r)^n - 1}$  in Eq. (30).

$$C_{\text{annual}} = \frac{C_{\text{TCI}} (1+r)^n}{(1+r)^n - 1} \quad (30)$$

where  $n$  is the system lifetime (year),  $r$  is the discount rate (%).

**Total capital investment** The total capital investment ( $C_{\text{TCI}}$ ) is determined by the purchasing cost and additional costs which are direct and indirect costs for the engineering, procurement, and construction (EPC) of the equipment. This cost can be expressed as a fraction of the purchased cost of equipment, including free-on-board (FOB) costs. The derivation of this equation can be outlined as below.

The bare module cost ( $C_{\text{BM}}$ ) is the sum of direct and indirect purchased costs for each piece of equipment ( $C_P$ ).

$$C_{\text{BM}} = \alpha_1 \cdot C_P \quad (31)$$

where  $C_P$  is purchased equipment cost ( $\text{\$/year}$ ), and  $\alpha_1$  is assumed to be 1.5.

Total bare module cost ( $C_{\text{TM}}$ ) is calculated as a fraction of  $C_{\text{BM}}$  with a constant value of  $\alpha_2$ .

$$C_{TM} = \alpha_2 \cdot \sum C_{BM} \quad (32)$$

where  $\alpha_2$  is assumed to be 1.18.

Grassroots cost ( $C_{GR}$ ) includes the costs for site development, auxiliary buildings, off-sites, and utilities.

$$C_{GR} = C_{TM} + 0.3 \cdot C_{BM} \quad (33)$$

Thus, total capital investment ( $C_{TCI}$ ) is:

$$C_{TCI} = C_{GR} + 0.15 \cdot C_{TM} \quad (34)$$

Substitute Eq. (12) and (13) into Eq. (14),

$$C_{TCI} = \alpha_1 \cdot C_P \cdot (1.48 + 0.5\alpha_2)$$

The capital cost for each equipment varies with its maximum power production or consumption rate, except for the hydrogenation and dehydrogenation reactors. As limited information for the procurement cost of these reactors was available, the costs for both reactors were estimated by fitting data within the equations in Ref.<sup>18</sup>, which is a function of equipment sizes and maximum power consumption for DBT and PDBT. The specific cost of the reactor is a function that has been linearized by multiplying the exponential factor used in the equation, and the cost of the reactors is then adjusted based on the relative ratio of STY of the LOHC with the STY of DBT-PDBT.

The capital cost of the hydrogenation reactor is

$$C_{hydro} = \frac{4261 P_{max} STY_{DBT}}{STY_{carrier}} \quad (35)$$

The capital cost of the dehydrogenation reactor is

$$C_{dehydro} = \frac{4683 P_{max} STY_{DBT}}{STY_{carrier}} \quad (36)$$

where  $P_{max}$  is the maximum power input/output of the equipment.

The capital and operating costs of each unit component are available in the Supplementary file (Table S4) and are estimated by multiplying by an additional cost factor of 2.455 for electrolyser, hydrogenation and dehydrogenation reactors, and hydrogen storage tanks. The costs for the solar PV and hydrogen dispensation units include the additional costs related to the EPC.

**Operating cost** The fixed operating cost includes the O&M cost of all equipment except for the solar PV system and PEM electrolyser. It is assumed to be 4% of the total capital cost per year.

The variable operating cost is the total electricity cost for optimal scheduling of the HRS, including the electricity consumed by water electrolysis and other system components. This cost is associated only with grid-related electricity inputs.

$$C_{operating, variable} = \frac{\text{Total electricity cost}}{\text{Total hydrogen production per year}} \quad (37)$$

## Scenario analysis

The scenario analyses were performed to identify the possible impacts of the changes in electricity supply sources, the selection of LOHC materials, and fluctuations in renewable energy prices on the performance and cost of the HRS.

The use of different LOHC materials is only considered in Scenarios 2 and 3, under the same analytical and modelling framework. The selected LOHC pairs in Table 3 differ in terms of the chemical structure, physical-chemical properties, and heat requirements for the dehydrogenation process.

### Scenario 1: electricity supply sources

Scenario 1 evaluates the behaviour of the hydrogen production and storage units when the electrolyser is powered by various electricity supply sources. There are two main electricity supply sources to be considered, which are a) an onsite solar PV system and b) existing power plants. The base case analysis was conducted using DBT/PDBT pairs as LOHCs.

#### Solar electricity only

When an onsite solar PV system is installed and connected to the electrolyser, hydrogen production is constrained to daily and seasonal variations of sunlight hours. The fluctuation in solar irradiation may result in insufficient solar energy generation. Consequently, hydrogen storage technologies are required to balance hydrogen production and demand throughout the year. When solar energy is not available or cannot meet the hourly electricity supply to the electrolyser, hydrogen is regenerated through the dehydrogenation process. Figure 8 illustrates the hydrogen production rate for solar-powered electrolyser and hydrogen charging/discharging rate for the hydrogen storage unit as a function of time, which is measured in kWh/50 kg<sub>H2</sub> for scaling purposes<sup>34</sup>.

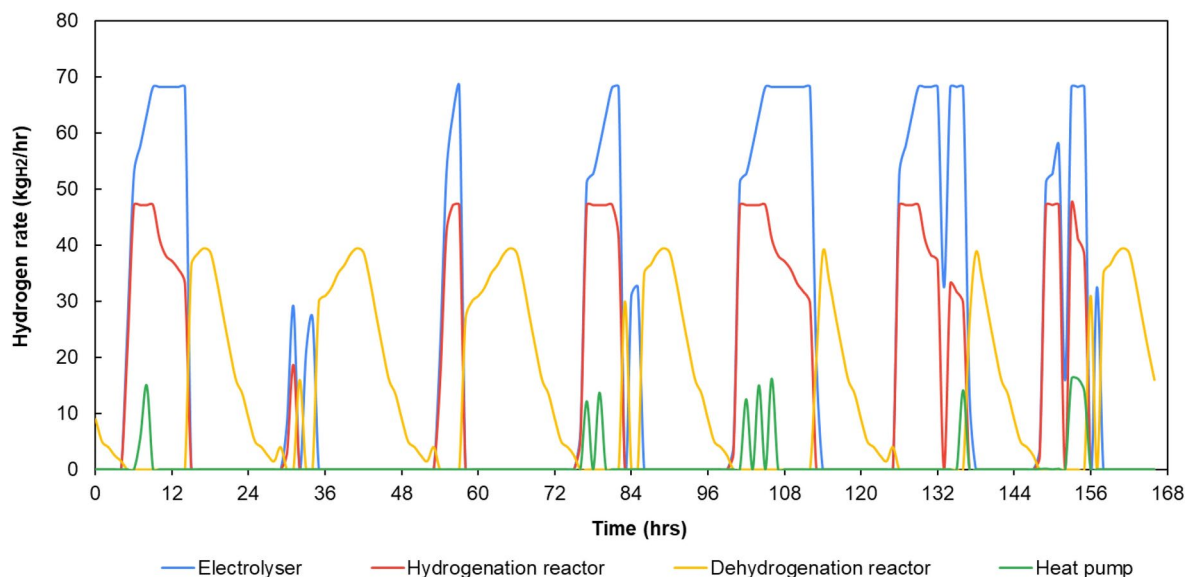


**Fig. 8.** Hydrogen production rate for solar-powered electrolyser and hydrogen charging/discharging rate for hydrogen storage unit from 1st to 7 January, considering the use of DBT/PDBT as LOHCs.

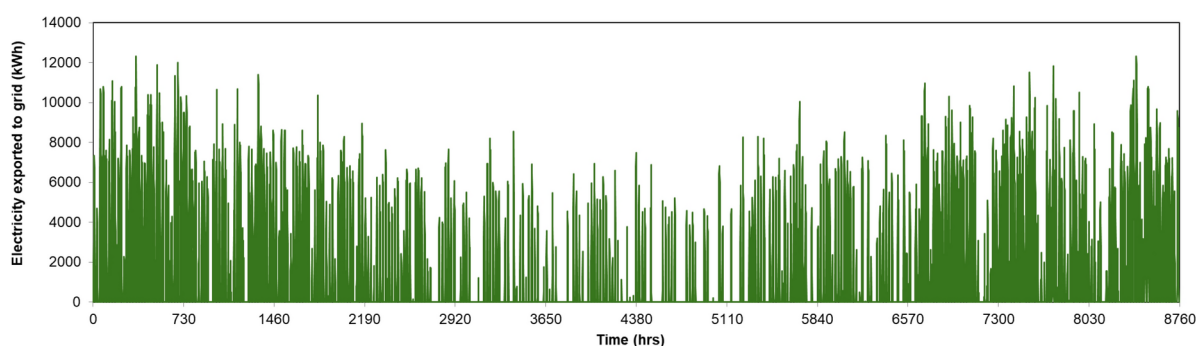


**Fig. 9.** Excessive solar electricity exported to the grid from 1 January to 31 December.

The hydrogenation reactor typically operates during the day until the hydrogenation storage tank reaches its design capacity of 47.16 kg<sub>H<sub>2</sub></sub>/hr. The dehydrogenation reactor is then activated to extract hydrogen from the hydrogenation storage tank to meet the peak demand at night or during blackout until the dehydrogenation storage tank reaches its design capacity of 39.5 kg<sub>H<sub>2</sub></sub>/hr. This could warrant a steady hydrogen supply, even when solar energy is unavailable. The energy usage of a heat pump to charge the thermal energy storage tank varies significantly throughout the day due to the variations in the amount of electricity generated from an onsite solar PV system, heat level in the thermal energy storage tank, and hydrogen demand.

The surplus electricity produced by the solar PV system is sold directly to the electricity grid. As shown in Fig. 9, the hourly export rate of solar electricity varies throughout the year. On average, the solar PV system produces more surplus electricity during summer (December to February) than it does during other seasons. During winter (June to August), there is no surplus solar electricity generated due to limited sunlight hours. Therefore, the hydrogen supply relies more on the dehydrogenation process than water electrolysis. This can lead to an increase in heat energy storage level as more heat from the thermal energy storage tank is used for the supplement of the dehydrogenation reactor (Fig. 10). The maximum heat storage level within the thermal heat storage can reach up to 26.3 MWh at 3735<sup>th</sup> hrs or 4 June.

The hydrogenation level of DBP is time-matched with electricity generation from an onsite solar PV system. However, there is a conflict between hydrogen storage levels in DBT and PDBT in separate hydrogenation and dehydrogenation reactors as shown in Fig. 11.

#### *Grid electricity only*

When electricity is purchased from a renewable power plant, the electrolyser can operate at its maximum capacity with a constant supply of electricity. Figure 12 shows the repetitive daily profiles for hydrogen production, hydrogenation, dehydrogenation, and heat pump with the use of grid electricity and DBT/PDBT as LOHCs. Notably, hydrogenation happens during midnight, while dehydrogenation occurs from noon until

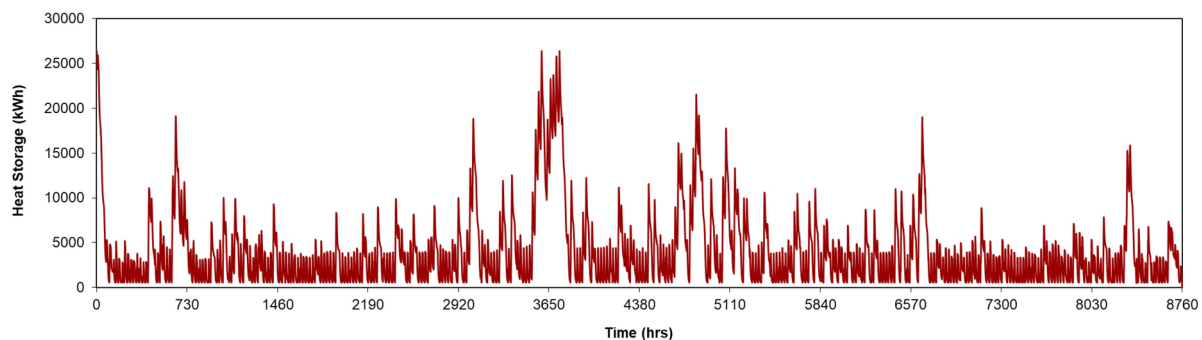


**Fig. 10.** Hourly heat storage level profiles for dehydrogenation reactor.

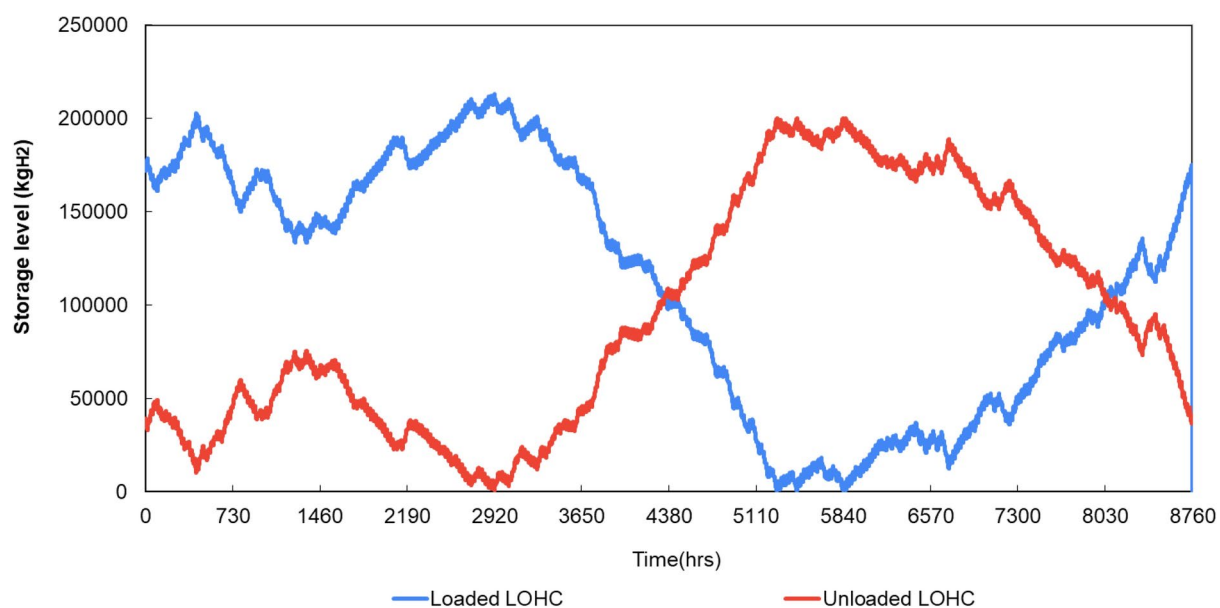


**Fig. 11.** The storage levels of hydrogen in DBT/PDBT in separate hydrogenation and dehydrogenation reactors.

early evening. During the first week of January, there is a conflict between the hydrogen production rate of the grid-connected electrolyser and the hydrogen discharging rate of the dehydrogenation reactor for a duration of three hours between the 86th and 90th hour in the late afternoon. The electrolyser's hydrogen production rate decreased, while the dehydrogenation rate remained constant in the dehydrogenation reactor. This is due to the grid electricity prices spiking to their highest levels throughout this period, as shown in Fig. 13. For assessing the impact of seasons, we have also looked at the system operations in two extreme weather conditions, i.e. January (peak summer), and July (peak winter) in Canberra. The Supplementary file provides the operation profiles (Section S3).

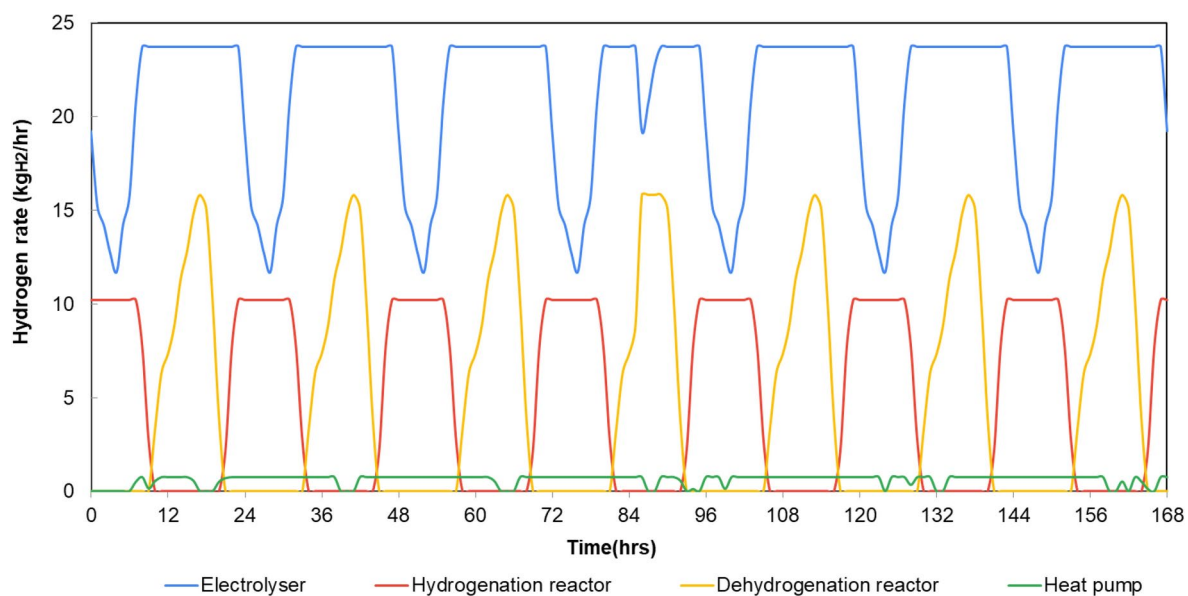
It is noteworthy that electricity prices remain constant across the seasons, so the overall magnitude of hydrogen production and storage does not change significantly. However, electricity prices tend to be more volatile during the summer due to higher sensitivity in electricity demand, leading to price spikes. As a result, hydrogen production may decrease during these peak periods, and the system may rely more on stored hydrogen reserves to meet demand. This effect is particularly evident in the January profile, where disruptions are observed, as explained above.

Figure 14 shows the thermal energy storage level for dehydrogenation. It is worth noting that the supply from the electricity grid remains constant over time due to its non-variable nature. Figure 15 shows hydrogen storage levels for the loaded and unloaded carrier tanks. Both graphs depict a repetitive pattern without any significant seasonal fluctuations.

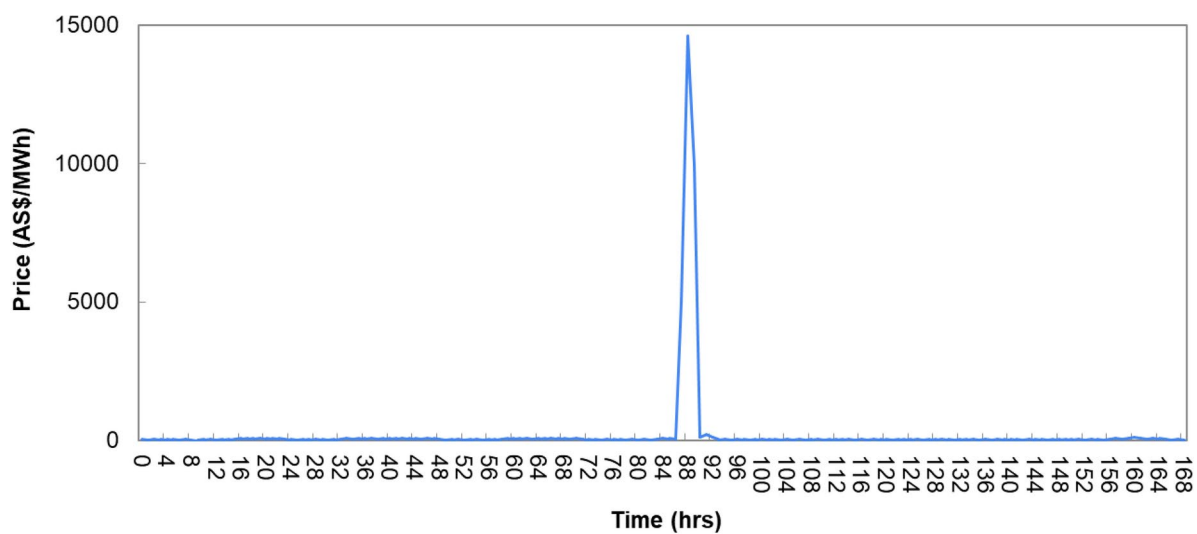
Figure 16 shows the relationship between energy usage of heat pumps and grid electricity prices for the optimal scheduling of the HRS. There is an inverse relationship between the heat pump energy usage and grid electricity prices. As the grid electricity prices decrease, the energy usage of the heat pump increases.

Figure 17 presents a time series graph for a grid-only scenario using NEC/DNEC as LOHC pairs. During a high electricity price event from the 86th to 90th hour, the hydrogen output from the electrolyser drops from





**Fig. 12.** Hydrogen production rate of the grid-connected electrolyser and hydrogen charging/discharging rate of the hydrogenation/dehydrogenation units from 1st to 7th January, considering the use of DBT/PDBT as LOHCs.



**Fig. 13.** Grid electricity prices from 1 to 7 January.

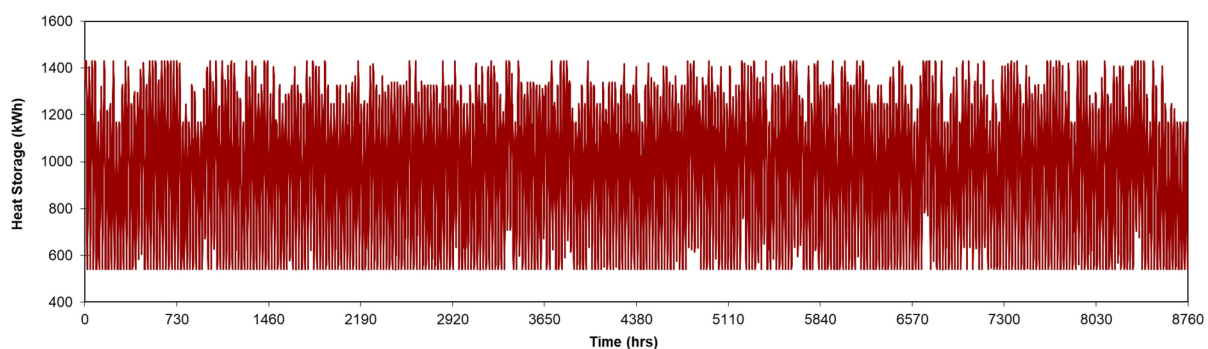


**Fig. 14.** Thermal storage level for dehydrogenation reactor.

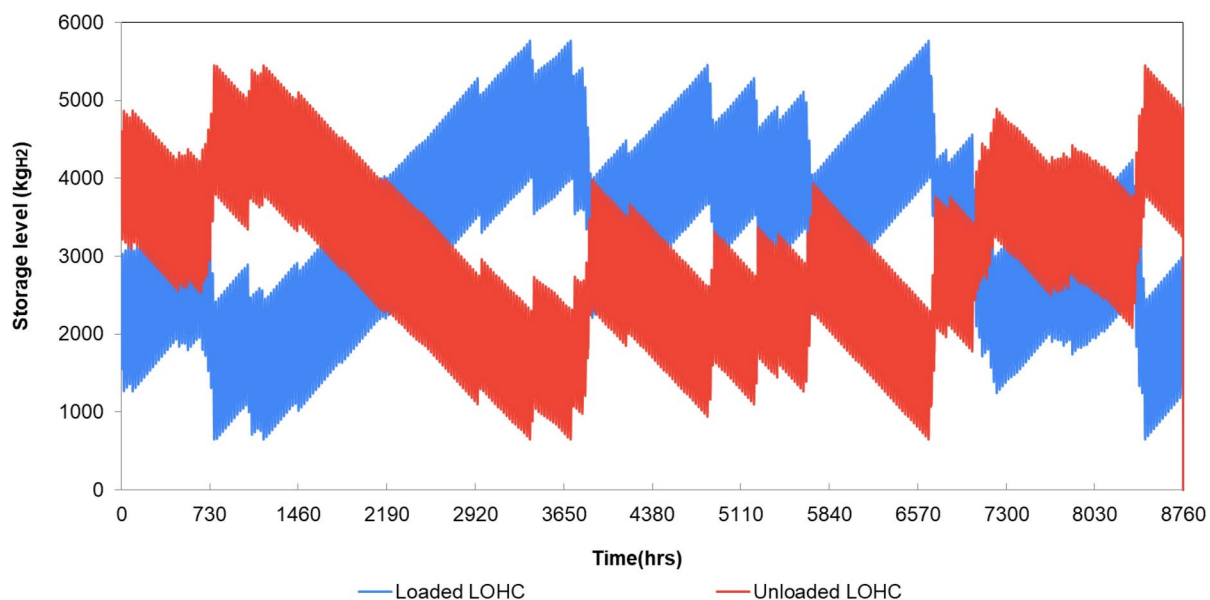


**Fig. 15.** Hydrogen storage levels in hydrogenation and dehydrogenation reactors when using DBT/PDBT pair as LOHC pairs.

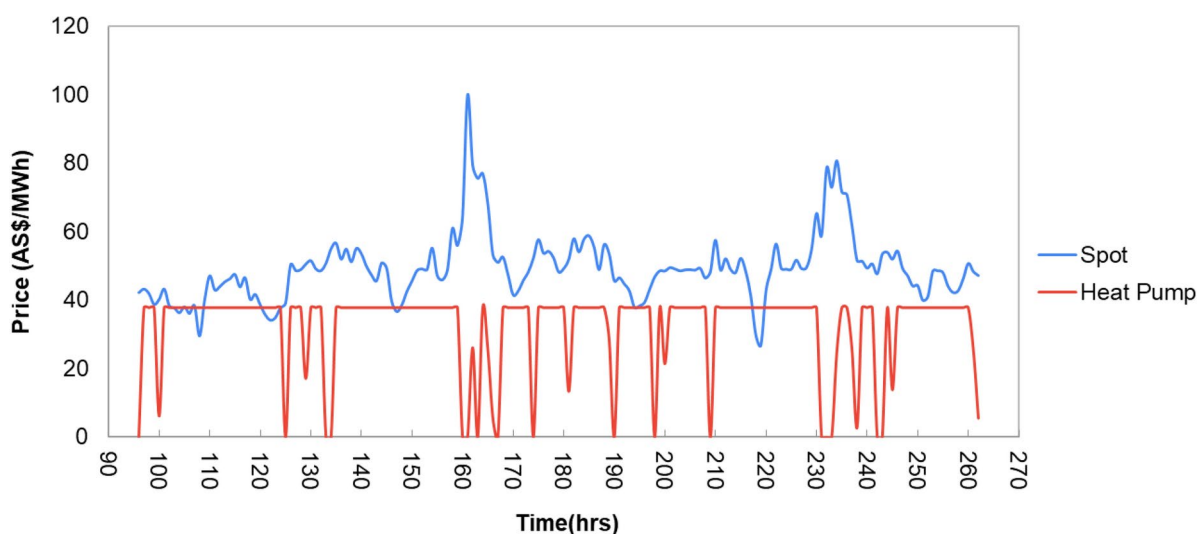


**Fig. 16.** The fluctuation in grid electricity prices and energy consumption of heat pump.

ca. 22 to 0, and the dehydrogenation reactor is utilised to meet the hydrogen demand. This suggests that it is important to consider the use of LOHC pairs under different scenarios to ensure the resilience and reliability of a HRS.

### Scenario 2: different LOHCs

Scenario 2 aims to examine the effect of using different LOHC pairs for hydrogen storage units on the capacity factor and economic feasibility. The potential LOHC candidates include DBT/PDBT, NEC/DNEC, TOL/MCH, and NAP/DEC pairs. These LOHCs have different structures and chemical and physical properties, which affect hydrogen storage density, heat requirements for dehydrogenation reaction, and equipment size. In this scenario, the sizing and cost of hydrogen dispensing unit are not taken into consideration.

The results of this scenario analysis show that the HPC is sensitive to the energy sources but not to the selection of LOHC materials. The HPC is calculated for the HRS with an onsite solar-driven electrolyser by comparing four different LOHC-based storage units. The use of a DBT/PDBT pair was chosen for the base case. For an HRS with an onsite solar-driven electrolyser (Fig. 18a), using MCH/TOL pair shows the lowest HPC value of A\$20.42/kg<sub>H2</sub> with dispensation and A\$19.34/kg<sub>H2</sub> without dispensation among all the LOHCs considered, while the use of the DBT/PDBT pair reflects the highest HPC value of A\$23.91/kg<sub>H2</sub> with dispensation and A\$22.82/kg<sub>H2</sub> without

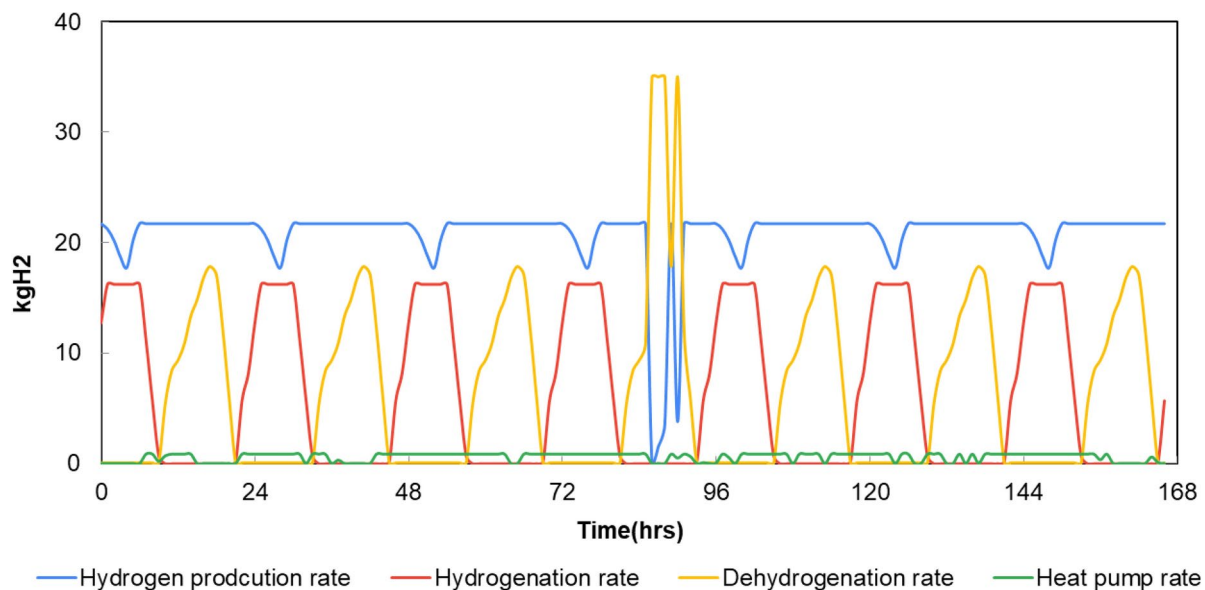


**Fig. 17.** Hydrogen production rate of the grid-connected electrolyser and hydrogen charging/discharging rate of the hydrogenation/dehydrogenation reactors from 1st to 7 January, considering the use of NEC/DNEC as LOHC pairs.

dispensation. For an HRS with a grid-connected electrolyser (Fig. 18b) the use of NEC/DNEC pair has relatively the lowest HPC value of A\$6.59/kgH<sub>2</sub> and A\$7.68/kgH<sub>2</sub> for with and without dispensation, respectively. When the cost of a hydrogen dispensing unit is included in the economic analysis of an HRS, the HPC increases by approximately A\$1.

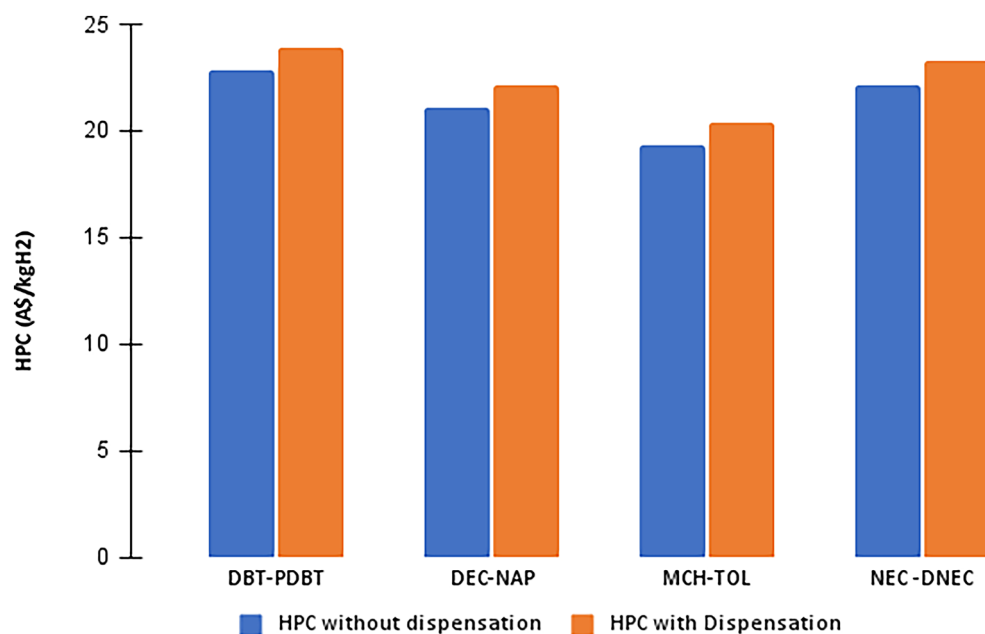
The HPC and capacity factor are highly dependent on the performance of energy sources. When considering solar power as the only electricity source for the HRS, the higher HPC is mainly due to the large equipment size required to accommodate intermittency. The lower HPC is due to the smaller equipment sizes and higher capacity factor of the equipment. The electrolyser size and electricity costs have a significant effect on the HPC.

For the solar-only case (Fig. 19a) NEC/DNEC pair requires the smallest size of all equipment, while DBT requires the largest. In contrast to the solar-only case, the size of the hydrogenation reactor is smallest for DBT and largest for NEC/DNEC pair (Fig. 19b). However, the size of the dehydrogenation reactor is considerably larger for NEC compared to other LOHCs, due to its very high STY of the dehydrogenation. The simulation results indicate a preference for utilising dehydrogenated stored hydrogen over producing hydrogen through electrolysis at very high electricity prices to meet the electricity demand, resulting in an increase in the size of the dehydrogenation reactor.

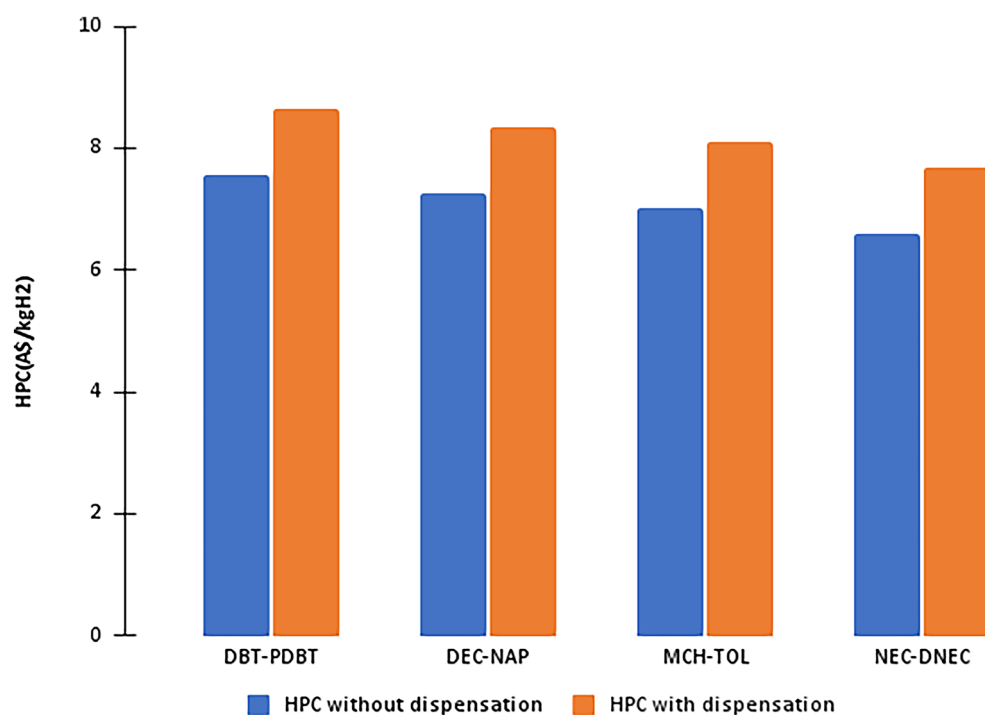
The capacity factor of electrolyser, storage reactors and heat pump are compared in accordance with the optimal results for the selected LOHCs. For solar-only case (Fig. 20a) the use of the NEC/DNEC pair shows the highest capacity factor of the electrolyser with the lowest solar-electrolyser ratio of 7.69. NEC has the lowest solar/electrolyser ratio and thus the lowest size of solar PV system, given that NEC electrolyser size is also the lowest. A low electrolyser size of NEC compared to others and a low solar electrolyser ratio gives the solar PV system the lowest sizing. DEC has the highest capacity factor of the hydrogenation reactor, while DBT has the highest capacity factor of the dehydrogenation reactor. The capacity factors of the heat pump remain the same across the four pairs of LOHCs.

For grid-only case (Fig. 20b), the electrolyser has a relatively high capacity factor when using either MCH/TOL or NEC/DNEC. The use of the DBT/PDBT pair results in the highest capacity factor of hydrogenation, while using MCH/TOL and DEC/NAP shows the highest capacity factor of dehydrogenation. Therefore, the capacity factor of all equipment in a grid-only case for all LOHCs is greater than in the solar-only case, especially the heat pump.

The cost breakdown for the equipment and utilities of the HRS model depends on the selection of LOHCs (Fig. 21). The electricity export and electrolyser contribute the most to the cost of the HRS model. In addition, the capital cost of the hydrogenation and dehydrogenation reactors is adjusted based on their relative ratios of space-time yield (STY). The higher the charging/discharging rate of the LOHC, the lower the volumetric capacity of the hydrogenation or dehydrogenation reactor required to produce the same amount of product, resulting in lower equipment costs. Thus, the STY values are used to compare the size and cost of hydrogenation and dehydrogenation reactors among different LOHCs. The same HRS model that uses MCH also requires the least capital cost for the hydrogenation reactor due to its high STY of the hydrogenation reaction. On the other hand, the use of NEC requires the lowest cost of the dehydrogenation reactor due to the high STY of dehydrogenation reactions. The cost of the hydrogen dispensing unit and the electricity it consumes are the same for all LOHCs as they have the same hydrogen demand.



(a)



(b)

**Fig. 18.** HPC for an HRS with (a) an onsite solar PV-driven electrolyser and (b) a grid-connected electrolyser, in a unit of A\$/kgH<sub>2</sub>. Blue bars indicate the HPC excluding the cost of the hydrogen dispensing unit; orange bars indicate the HPC including the cost of the hydrogen dispensing unit.

For grid- only case (Fig. 21b), the most dominant cost is the electricity cost of the hydrogen generation and storage unit, followed by the cost of the electrolyser cost and dispensation electricity. The cost of dispensation electricity and dispensing unit remain constant in both scenarios and are not affected by the selection of LOHCs. Electricity consumption has a significant impact on the total costs.

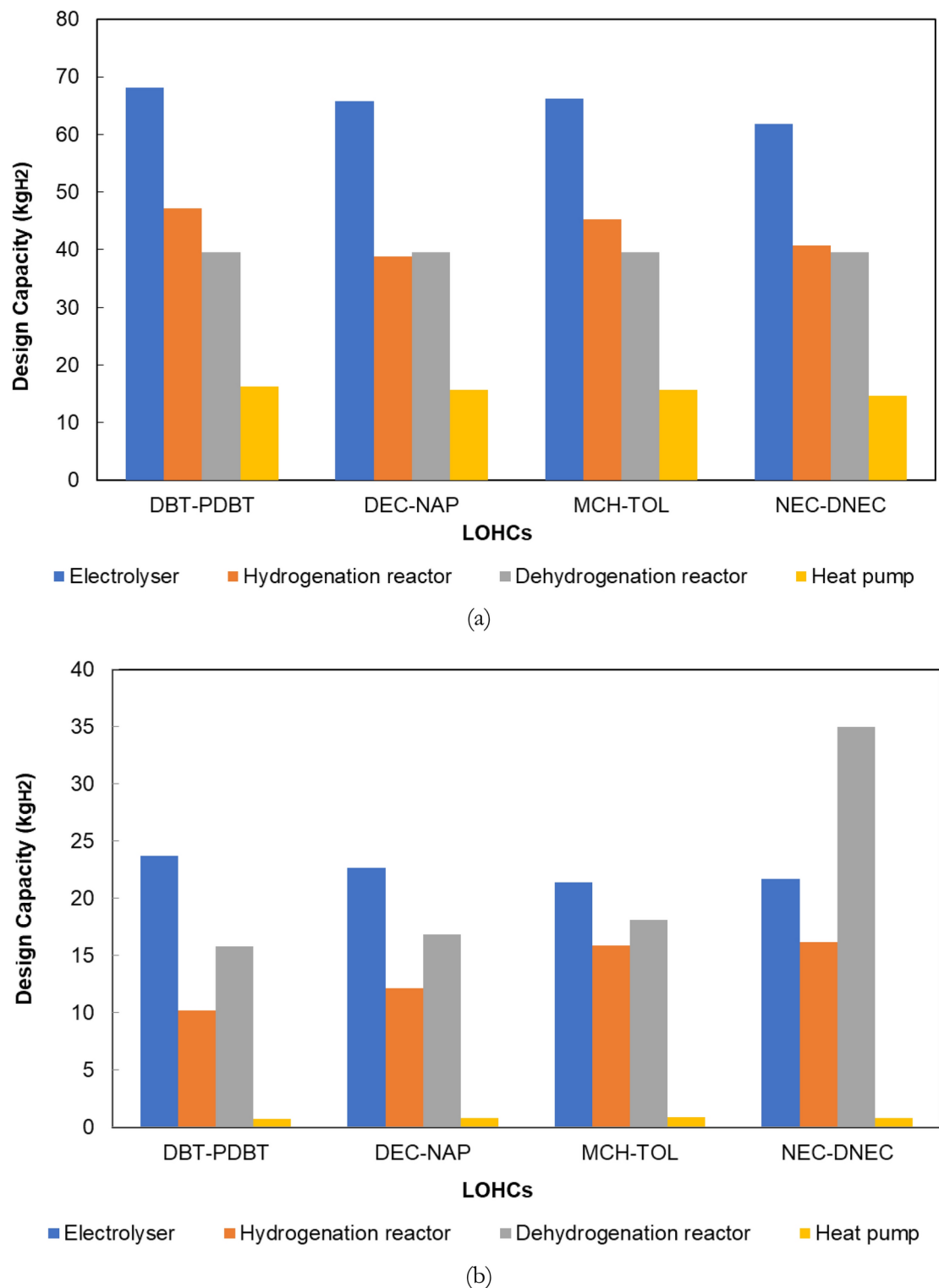


**Fig. 19.** Design capacity for different LOHC-based HRS with (a) an onsite solar PV-driven electrolyser and (b) a grid-connected electrolyser, in a unit of kgH<sub>2</sub>.

### Scenario 3: renewable energy prices

Scenario 3 assesses how the changes in renewable electricity prices may affect the HPC. The production of hydrogen is the most capital- and energy-intensive part of the hydrogen supply chain. Therefore, it is important to find out how much the capital cost of an onsite solar PV system would be to make the HPC more competitive in the market.



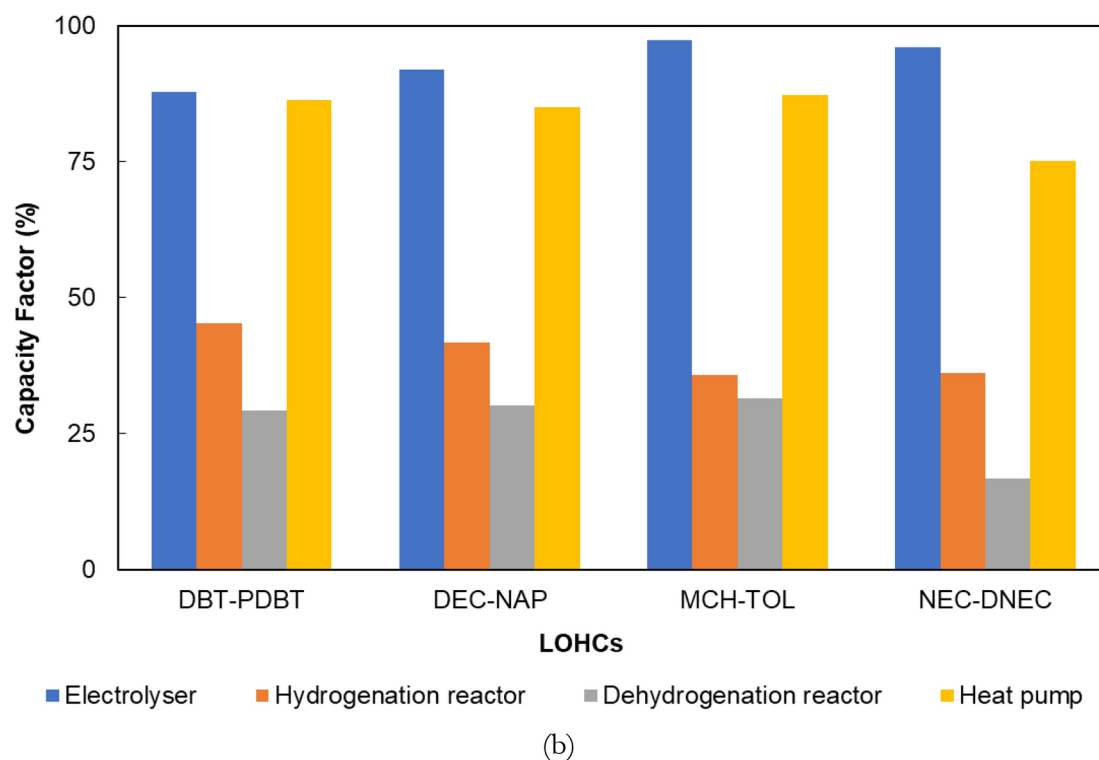
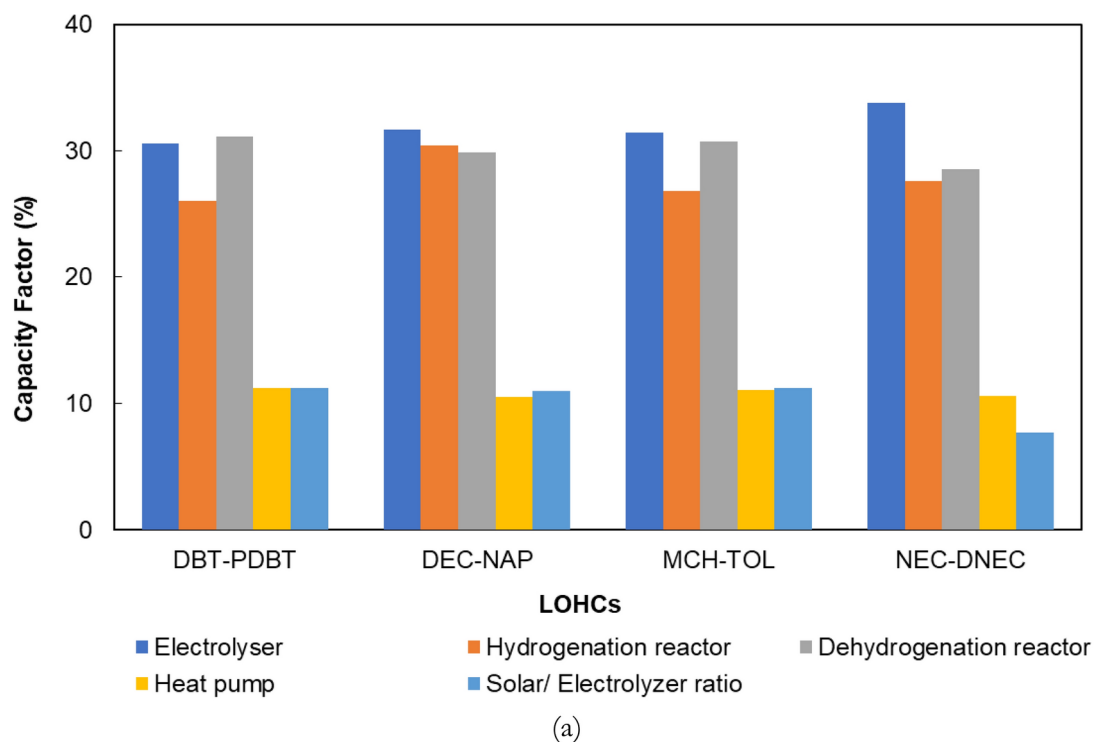


**Fig. 20.** Capacity factor of electrolyser, hydrogenation and dehydrogenation reactors, and heat pump for different LOHC-based HRS with (a) an onsite solar PV-driven electrolyser and (b) a grid-connected electrolyser.

The cost patterns for the different LOHC-based HRS are very similar when the capital cost of an onsite solar PV system varies. Figure 22 shows the HPC for different LOHC-based HRS without and with dispensation and compares the costs associated with solar PV prices. When the capital cost of an onsite solar PV system is A\$2000, the HPC without dispensation for DBT/PDBT pair has the highest value of A\$7.58 among these HPCs, while the HPC for NEC/DNEC has the lowest value of A\$6.62. The HPC values are shown in Fig. 22b and c are estimated

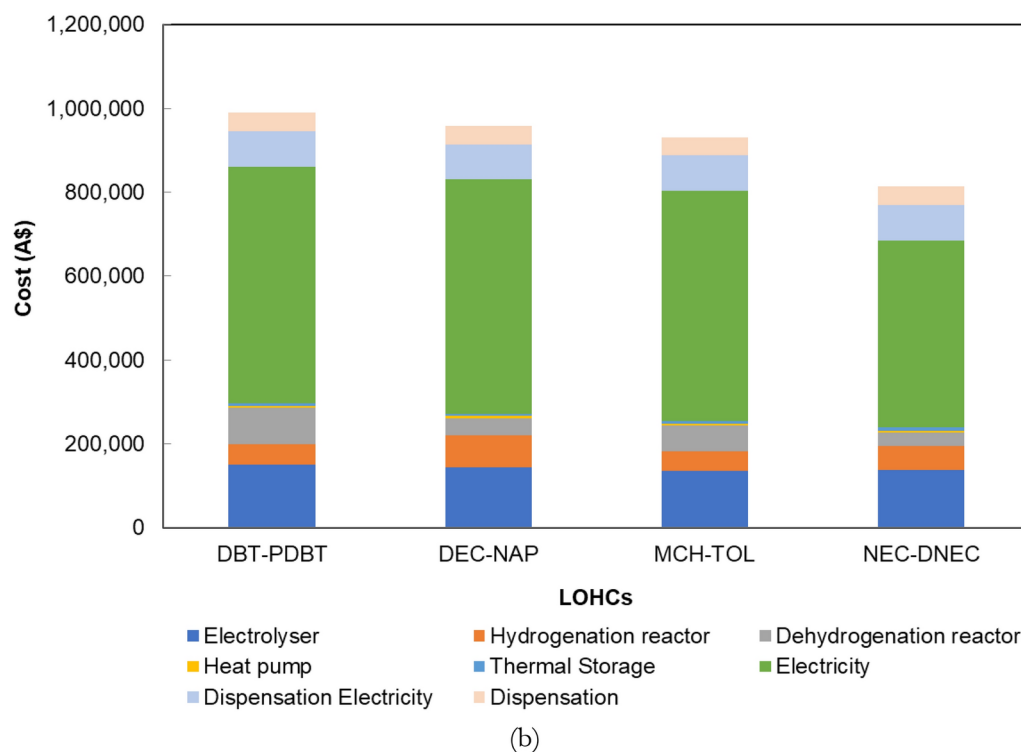
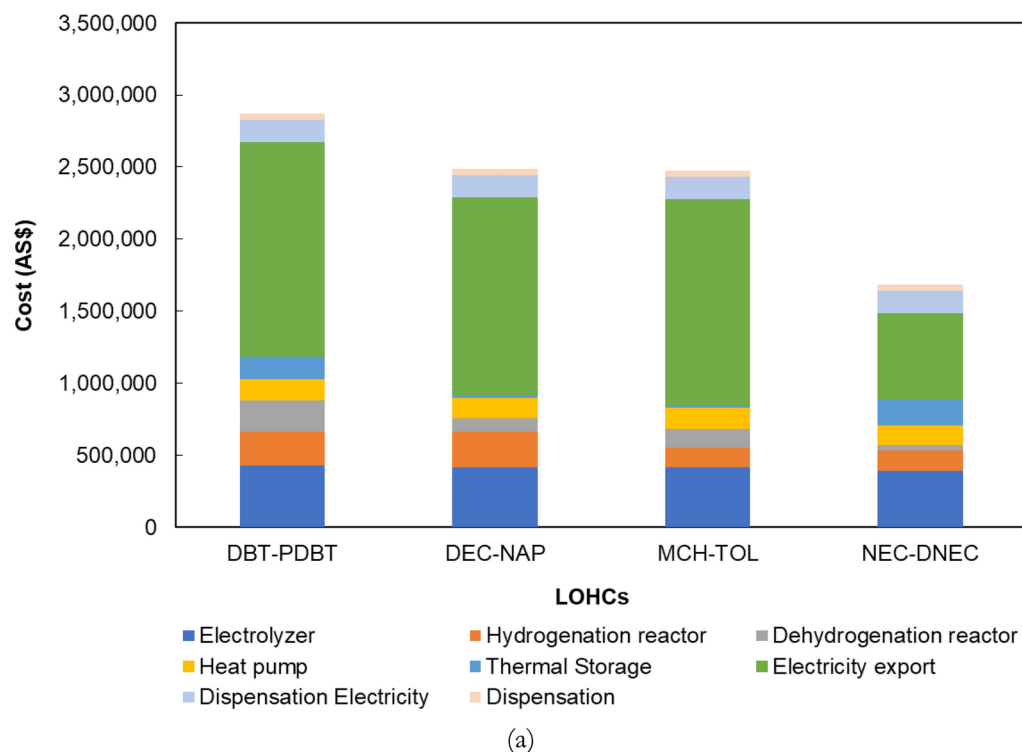


**Fig. 21.** The cost structure for equipment and electricity exported to grid of different LOHC-based HRS with (a) a solar PV-driven electrolyser and (b) a grid-connected electrolyser, in a unit of A\$.

based on the solar PV prices of A\$1500 and A\$1000 respectively, which have a similar pattern to Fig. 22a. The HPC remains almost constant when the solar PV price is increased from A\$1000 to A\$2000. When the cost of the hydrogen dispensing unit is included, the HPC increases by approximately A\$1 for all cases.

The variations in the capital and operating costs of all equipment as illustrated in Fig. 23 have a minor impact on HPC values.

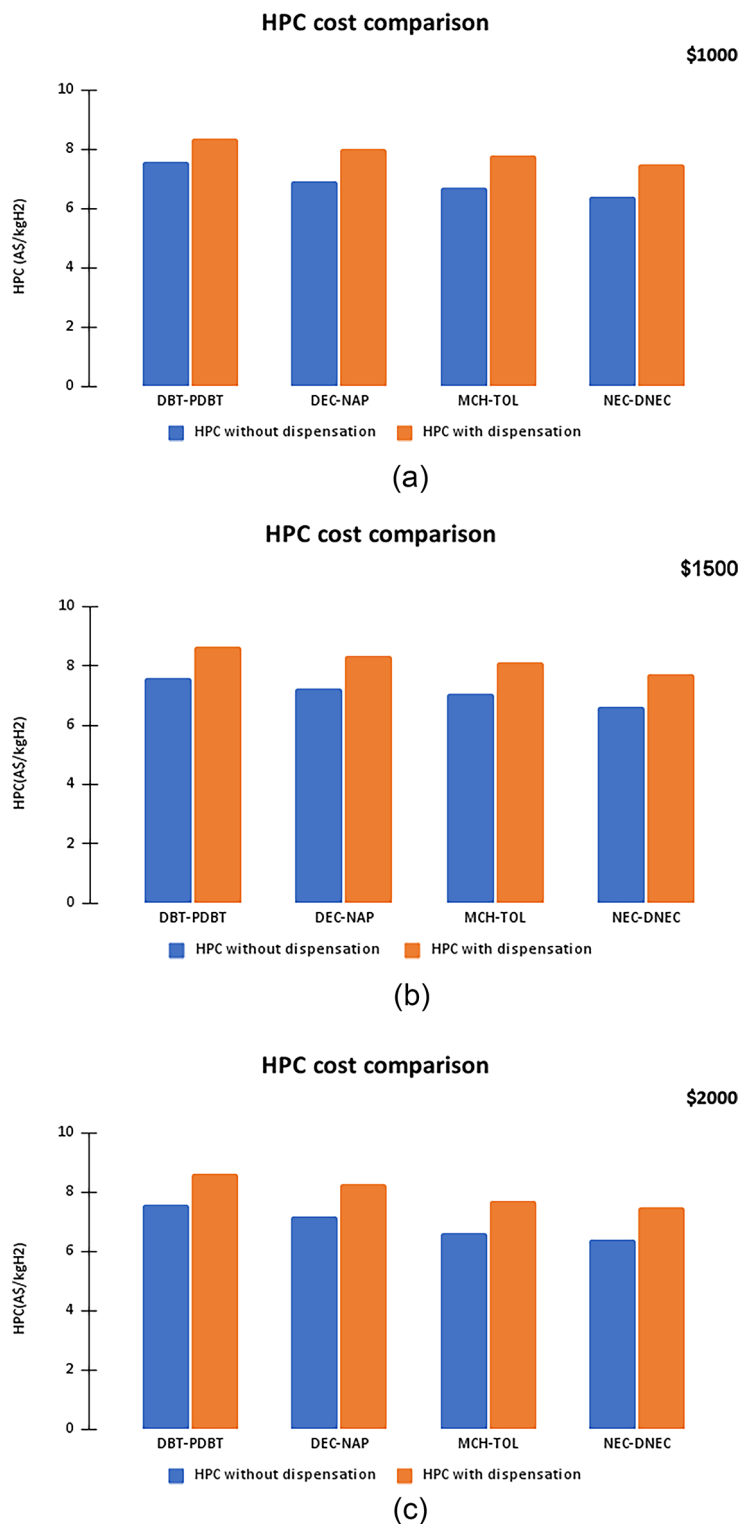


**Fig. 22.** HPC for different LOHC-based HRS without dispensation (blue) and with a dispensation (orange) when the capital costs of a standalone solar PV system are (a) A\$2000 (b) A\$1500 and (c) A\$1000, respectively.

The design capacity of the dehydrogenation reactor is more sensitive to the changes in renewable energy prices than other LOHCs when using NEC/DNEC as LOHCs. Figure 24 illustrates the design capacity of hydrogen production and LOHC-based storage units for different capital costs of an onsite solar PV system. The design capacity of each piece of equipment is similar for the use of the same LOHC as shown in Fig. 24a and b. However, the design capacity of the dehydrogenation reactor for NEC/DNEC with a solar PV price of A\$2000 is nearly double that of other LOHCs. While the sizes of the electrolyser and heat pump are very similar across

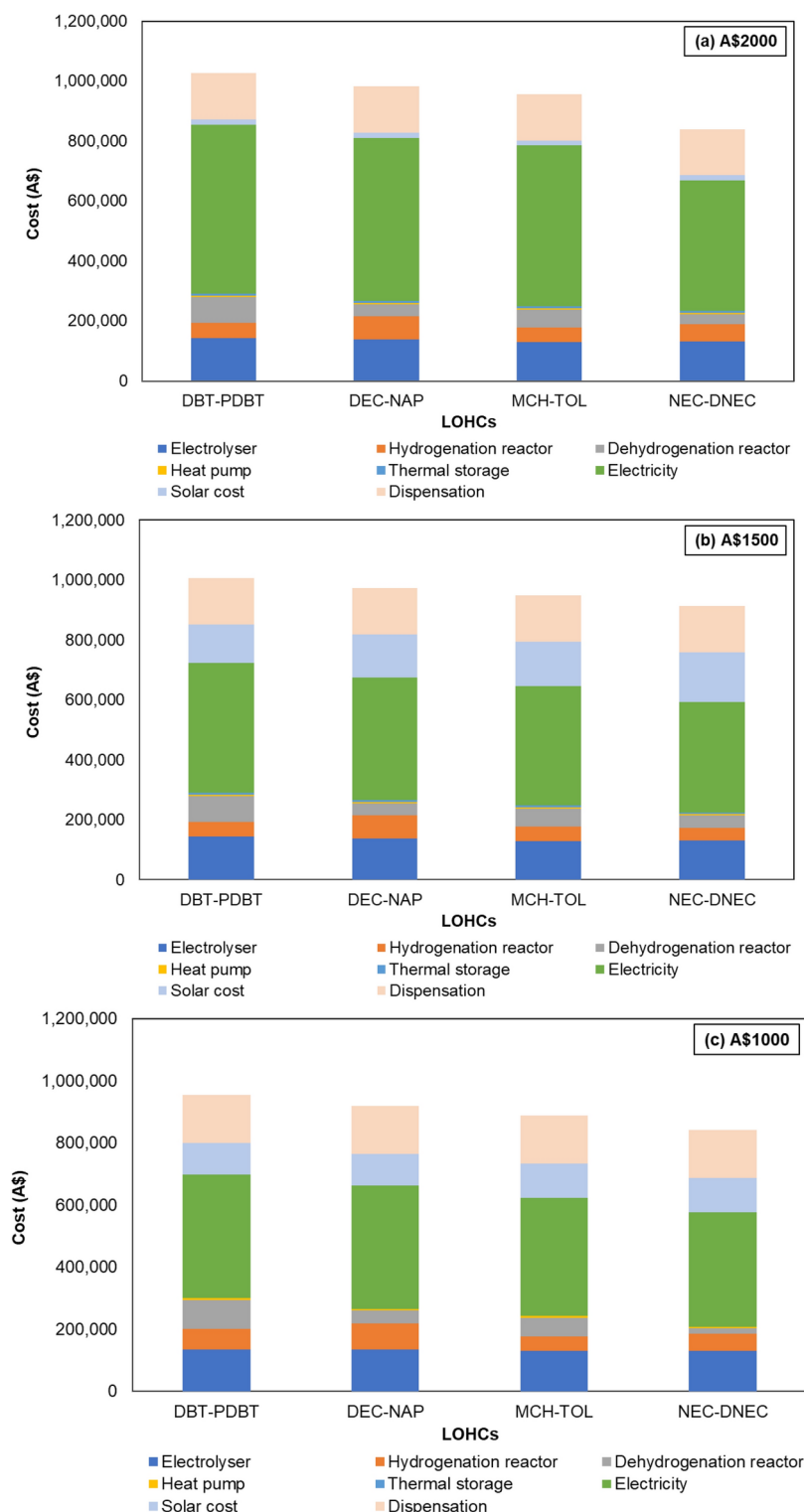


**Fig. 23.** The cost structure for equipment and electricity exported to the grid of different LOHC-based HRS when the capital costs of a solar PV system are (a) A\$2000 (b) A\$1500 (c) A\$1000 respectively.

different LOHCs, there is a noticeable discrepancy in the sizes of hydrogenation and dehydrogenation reactors. Figure 25 illustrates the energy consumption for different LOHC-based HRS for different scenarios.

In this study, the Sankey diagrams are used to visualise the energy flows, analyse the use of the electrical energy sources across the HRS, and identify the potential opportunities for energy efficiency improvement. The width of each energy flow stream in the diagrams is proportional to the actual amount of energy transferred into or out of the energy units per unit of time.

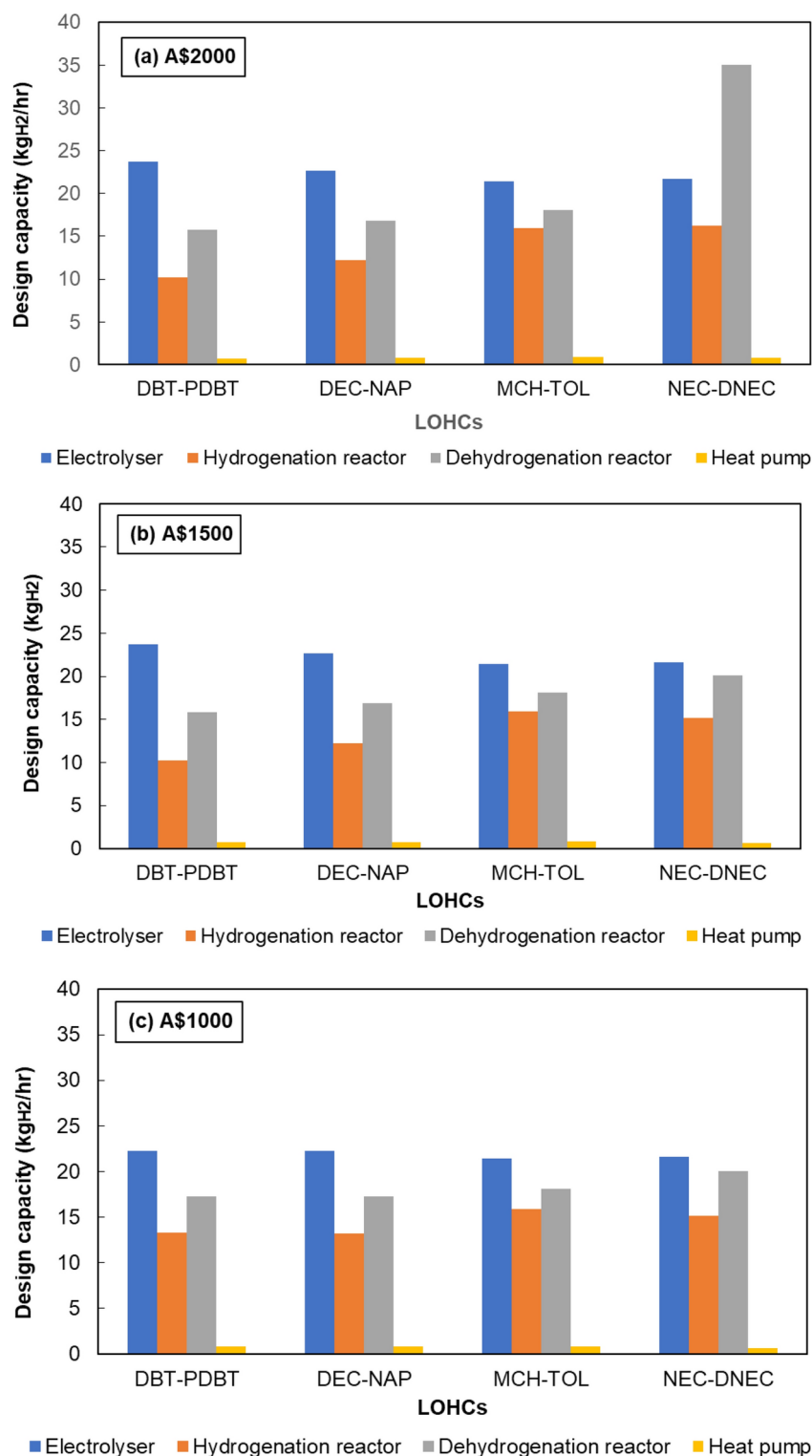


**Fig. 24.** Design capacity of hydrogen production and LOHC-based storage units when the capital costs of an onsite solar PV system are (a) A\$2000, (b) A\$1500 (c) A\$1000, respectively.

Solar energy is the primary energy source that provides electricity for the HRS system. Sankey diagram in Fig. 26 shows the flow of solar energy and its transformation across various physical equipment of the HRS. The PEM electrolyser is the main consumer of electricity, followed by the heat pump during the energy consumption stage. The solar PV output can provide enough energy required by the process and to export the excessive electricity generated to the grid. The dispensing units are powered by grid electricity to ensure that the chiller, compressor, and dispenser can still operate when solar electricity is not available.



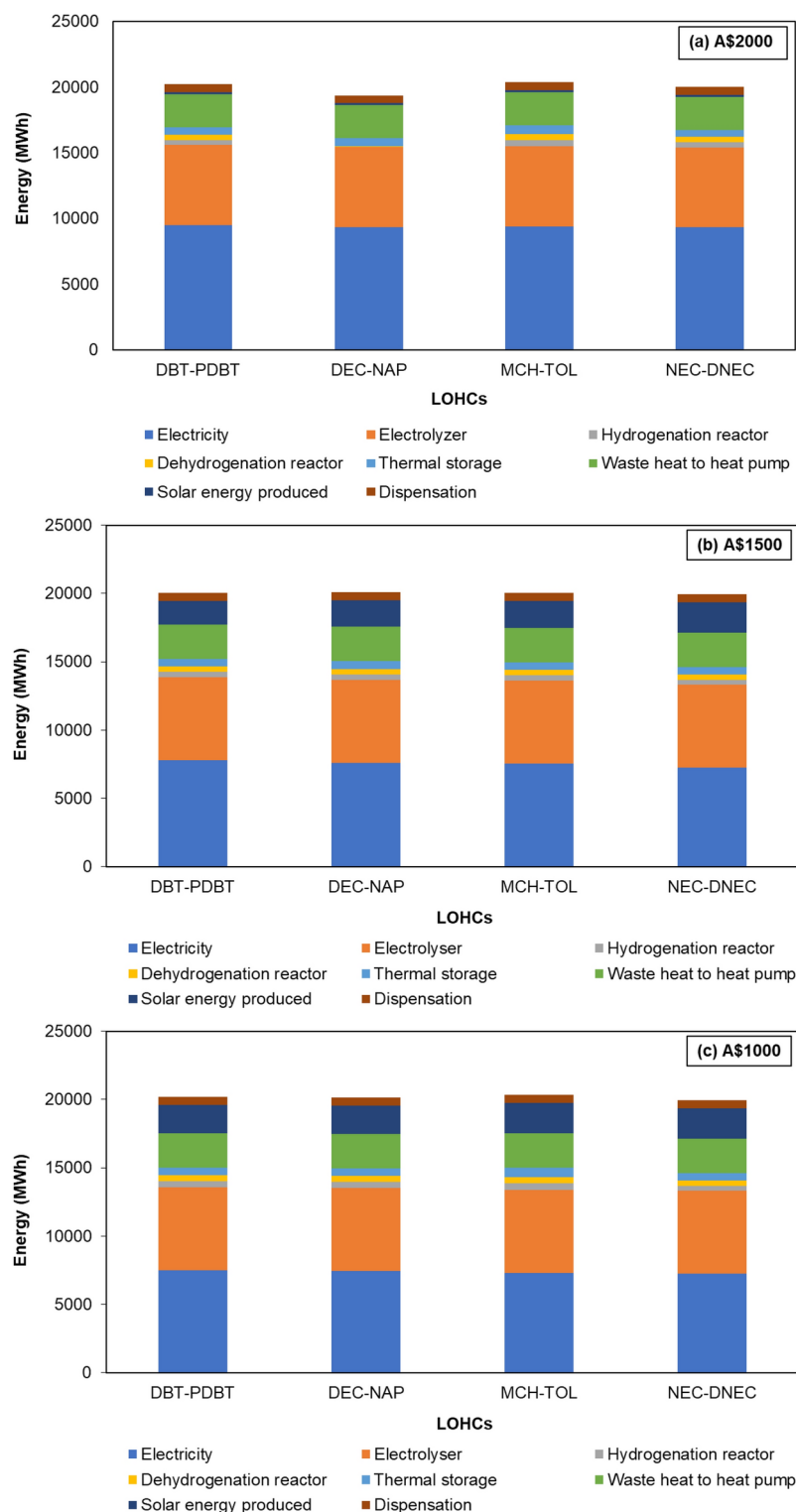


**Fig. 25.** Energy consumption for different LOHC-based HRS when the capital costs of an onsite solar PV system are (a) A\$2000, (b) A\$1500 (c) A\$1000, respectively.

The amount of waste heat and energy loss generated by the electrolyser accounts for approximately 30% of the total electrolyser energy content. The energy resulting from the conversion of waste heat is partially captured by a heat pump and transferred to a thermal energy storage tank, which is identified as a viable solution to address the issue of intermittency in the energy supply. However, the challenge at this stage is the energy losses, which are output as the energy losses in the form of heat produced in the PEM electrolyser and thermal energy storage tank.

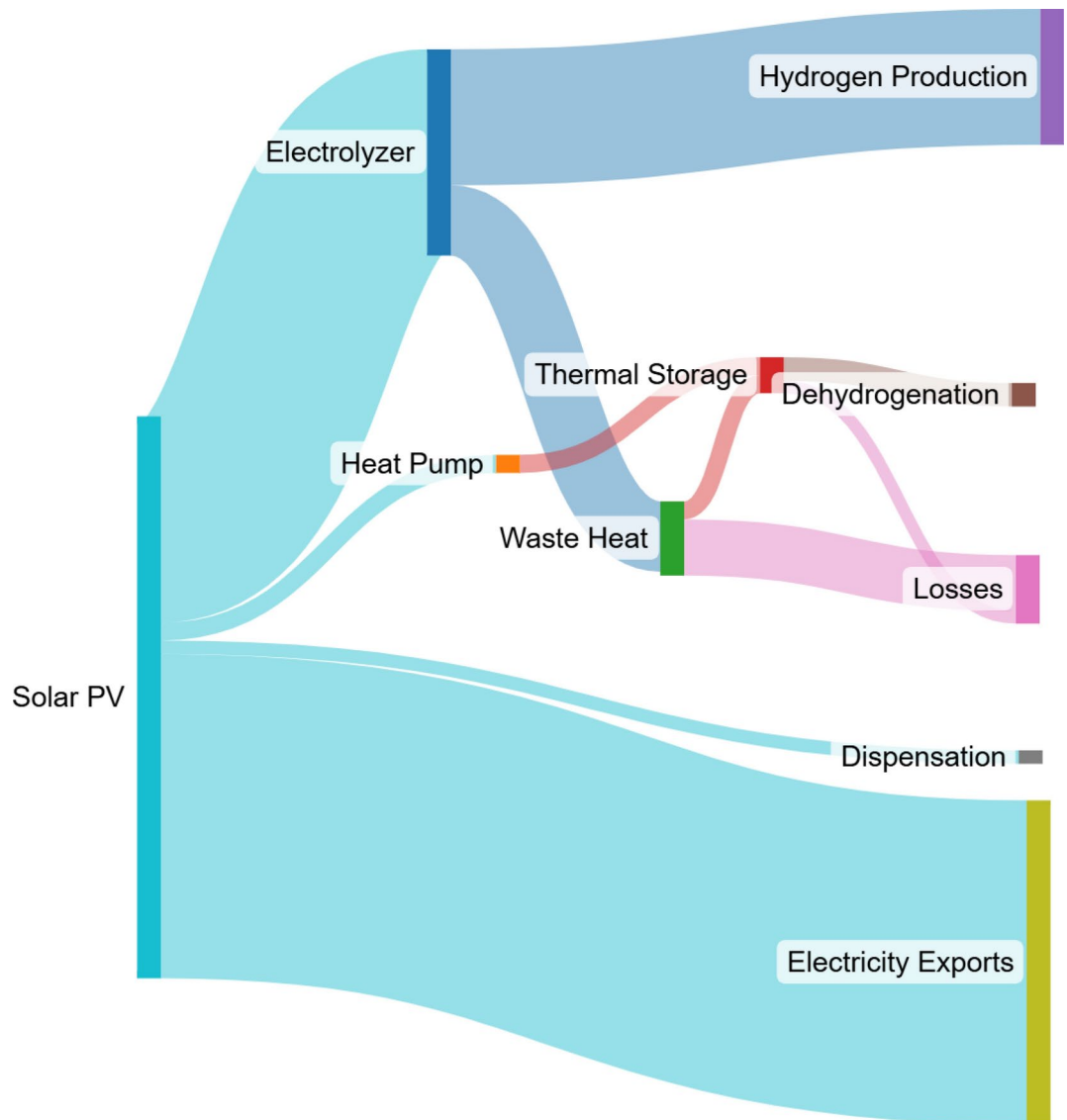


**Fig. 26.** Sankey diagram of solar electricity flows and losses for the HRS.

The electricity from the grid and onsite solar PV systems are directly used for hydrogen production and heat management. Figures 27 and 28 show the energy flows and usage across the HRS powered by both electricity sources, which have similar patterns. It is clear that the electrolyser is a major electricity consumer for both solar-only and grid-only cases. The energy leaves the electrolyser accounts for 85–94% of total electricity consumption. However, the heat pump consumes only a small portion of the electricity. As the coefficient of performance (COP) of the heat pump system is 2, the waste heat delivered to the thermal energy storage tank is almost twice the heat pump energy content, resulting in more energy losses than the solar-only case. Further losses that occurred at the end could be identified as an opportunity to improve energy efficiency and solve the intermittency in renewable electricity supply in the future.

One major difference between the two cases is the relative energy content sizes in the respective equipment, with the solar-only case being larger. This is due to the low-capacity factor of the solar-only case, resulting from the intermittency of solar electricity generation, compared to the grid-only case. This means that the larger sizes of the electrolyser, storage reactors, heat pumps, and thermal energy storage are required to accommodate the intermittency. However, the waste heat content in the aggregate is equal in both cases because of the same aggregated amount of hydrogen production.

## Conclusions

In this paper, the techno-economic analysis of an HRS is conducted. The optimal results indicate that using NEC/DNEC pair as a hydrogen carrier for the application of hydrogen refuelling stations is commercially favourable. A new technical model for the process chain of HRS has been analysed, optimally sized and simulated under two different scenarios with varying electricity inputs. The entire HRS chain has been evaluated using different

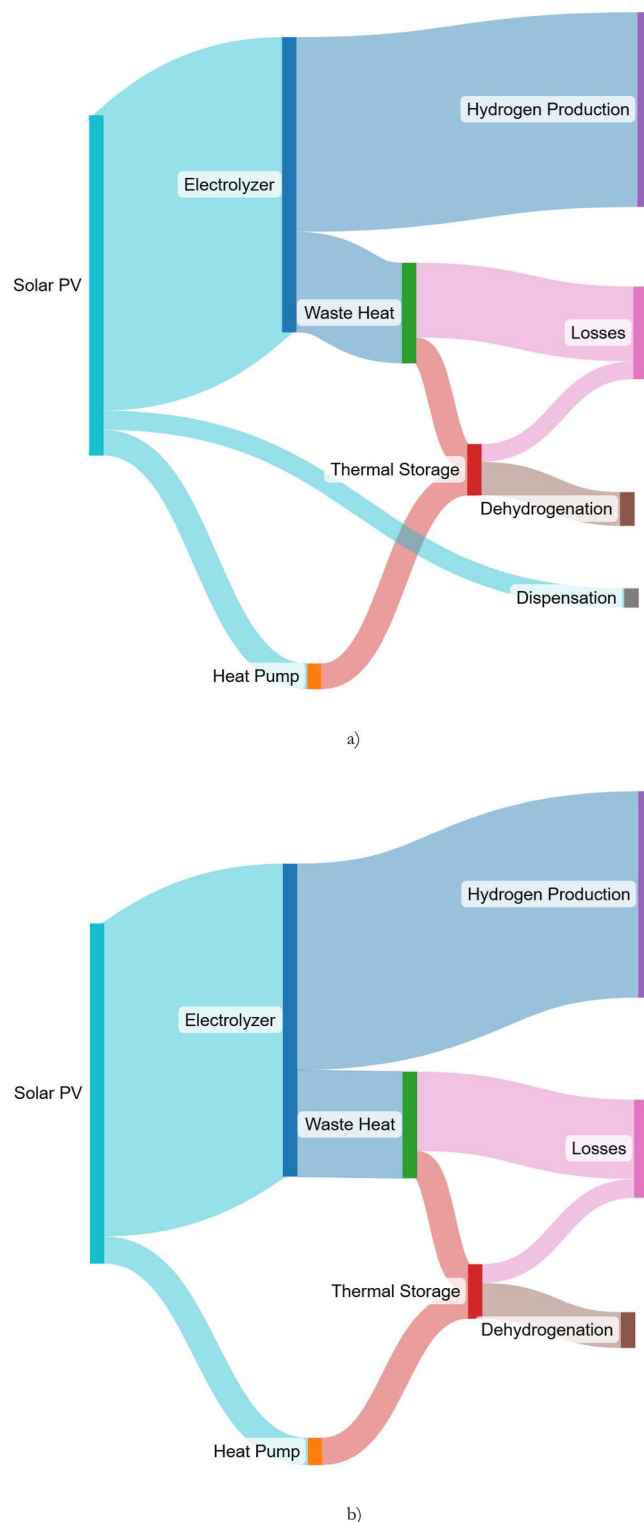


**Fig. 27.** Sankey diagram of solar energy flow and loss excluding electricity export.

LOHC storage systems in terms of technical and economic aspects. Total annualised cost is determined by technical and economic factors, such as renewable energy source prices and capital expenditure. The results show significant variation in the sizing and scheduling of the HRS system depending on the electricity inputs and LOHCs used. A grid-connected electricity for the HRS is techno-economically better rather than using solar PV for electricity input for all LOHCs based on the lower HPC and higher CF of the former. MCH has the

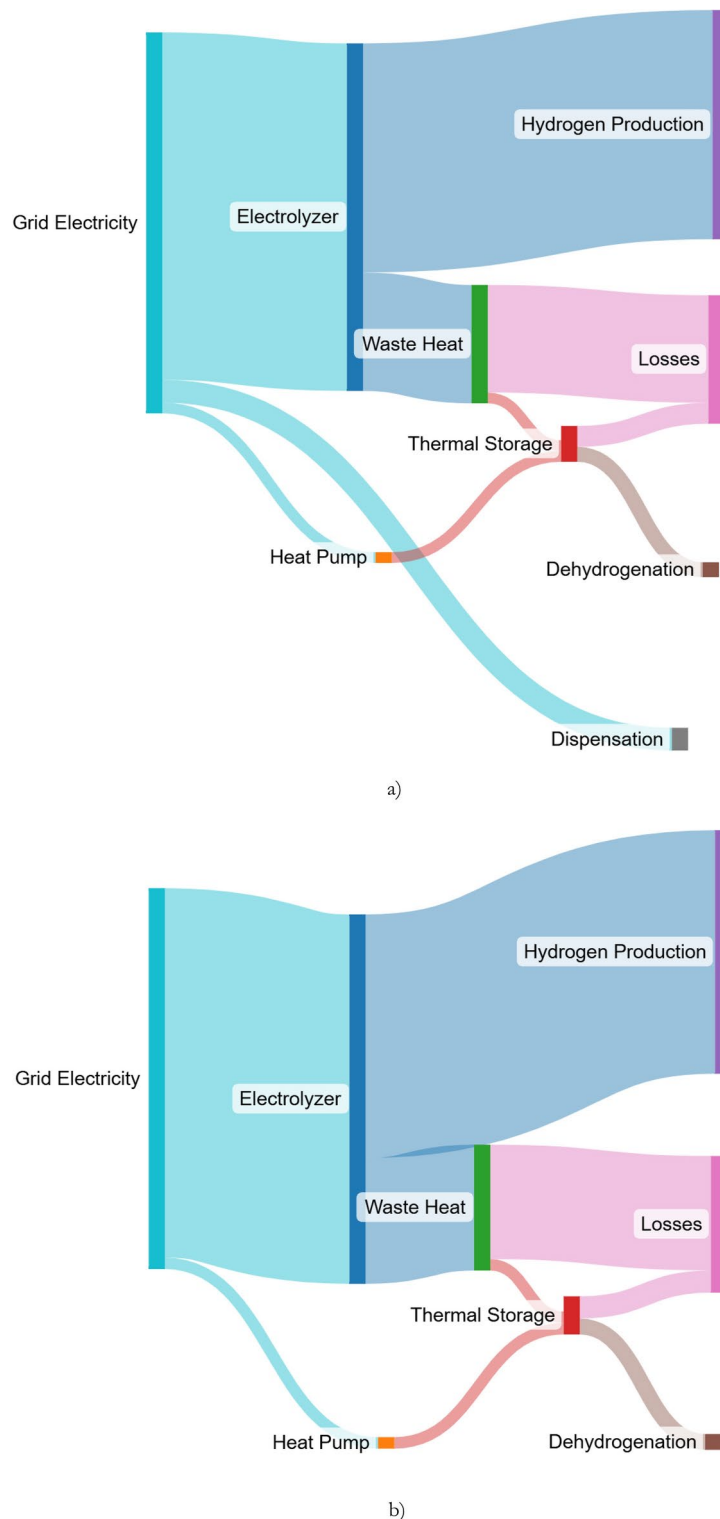


**Fig. 28.** Sankey diagram of grid electricity flows and losses for HRS.

lowest HPC with solar PV electricity input, while NEC has the lowest HPC with grid-connected electricity input. However, each LOHC storage system has different sizing and capacity factors with the same inputs, making it unclear which LOHC is the best option for integrating LOHC storage into an HRS. Different applications under varying conditions may warrant the use of a different LOHC. Nevertheless, NEC appears to be more effective at accommodating intermittency for an HRS application, making it a suitable LOHC for stand-alone renewables integrated hydrogen process chain. MCH is also a viable option for high intermittency in the renewables-integrated hydrogen process chains due to its hydrogenation STY.

The heat internalisation mechanism and overall hydrogen process chain presented in the paper demonstrate robust and resilient behaviour. This requires further investigation and more detailed technical consideration in future studies.

The modelling approach of the paper was contextualised within certain constraints, including uncertainty in cost reduction due to technological advancement and economies of scale, as well as a lack of data availability and literature on hydrogen demand behaviour. As a result, this study utilised conservative estimates for costs in a particular environment and optimised the entire HRS chain to obtain a pessimistic value for HPC. Consequently, some cost inputs were intentionally set to high values. However, with a better understanding of the behaviour of different inputs used in the modelling, it is possible to obtain lower HPC values in the future.

The LOHC storage technology has the potential to significantly impact the uptake of hydrogen refuelling infrastructure and the adoption of HFCVs globally. By providing a suitable, cost-effective means of hydrogen storage for HRS, LOHC technology can help to address some of the key challenges in the development of a hydrogen economy, such as the cost and availability of hydrogen. However, future work is needed to improve the efficiency and understanding of the LOHC integrated hydrogen process chain, including the internalisation of heat and the selection of the appropriate LOHC. With continued research and development, the LOHC storage technology can play a vital role in creating a more sustainable and viable transportation system based on hydrogen fuel.

## Data availability

The input data is provided within the paper or in the supplementary file.

## Glossary

Abbreviations	ACC	Annual capital costs
ACT		Australian capital territory
CAPEX		Capital expenditure
CEC		California energy commission
CF		Capacity factor
COP		Coefficient of performance
CSTP		Concentrated solar thermal power
DBP		Dibenzyltoluene
DEC		Decalin
DNEC		Dodecahydro-N-ethylcarbazole
HFCEV		Hydrogen fuel cell electric vehicle
HRS		Hydrogen refuelling station
HTF		Heat transfer fluid
HPC		Hydrogen production cost (same as levelised cost of hydrogen)
LHV		Lower heat value of hydrogen
LOCH		Liquid organic hydrogen carrier
MCH		Methylcyclohexane
NAP		Naphthalene
NEC		N-ethylcarbazole
NREL		National renewable energy laboratory
$OPEX_{\text{fixed}}$		Fixed operating expenditures
$OPEX_{\text{variable}}$		Variable operating expenditures
$P_{\text{max}}$		Maximum power
PDBT		Perhydro-dibenzyltoluene
PTES		Pumped thermal energy storage
PEM		Proton exchange membrane
PV		Photovoltaics
SAM		System advisor model
TAC		Total annualised cost
TCI		Total capital investment
TOL		Toluene
TES		Thermal energy storage
TTES		Thermocline thermal energy storage
Notations	$y_{i,j}$	Hydrogen production rate
	$u_{i,j}$	Hydrogenation rate
	$v_{i,j}$	Dehydrogenation rate
	$x_{i,j}$	Hydrogen demand rate
	$m_{1,i,j}$	Loaded tank mass level
	$m_{2,i,j}$	Unloaded tank mass level
	$i$	Hour of the day (1–24)
	$j$	Day of the year (1–365)
	$E$	Specific electricity consumption of the electrolyser
	$W$	Work done on the heat pump
	$Q_c$	Low temperature heat source

$Q_h$	High temperature heat source
$H$	Enthalpy of the reaction
$x_1$	Stoichiometric mass ratio of unloaded carrier to hydrogen
$x_2$	Stoichiometric mass ratio of loaded carrier to hydrogen
$\eta_{\text{electrolyser}}$	Electrolyser efficiency
$\varepsilon$	Heat exchanger effectiveness
$\mu_2$	Degree of dehydrogenation

Received: 10 July 2024; Accepted: 20 February 2025

Published online: 25 March 2025

## References

- Hannah Ritchie. Cars, planes, trains: where do CO<sub>2</sub> emissions from transport come from? <https://ourworldindata.org/co2-emissions-from-transport> (2020).
- H2stations.org by LBST. Statistics: Hydrogen Infrastructure (2022).
- Rajeev Bhalla. How markets determine the price of Hydrogen. <https://www.mvsengg.com/blog/how-markets-determine-the-price-of-hydrogen/#:~:text=Hydrogen%20price%20to%20the%20customer,of%20price%20to%20the%20customer.>
- Basile, A., Liguori, S. & Iulianelli, A. 2-Membrane reactors for methane steam reforming (MSR). In *Membrane Reactors for Energy Applications and Basic Chemical Production* (eds Basile, A. et al.) 31–59 (Woodhead Publishing, 2015). <https://doi.org/10.1016/B978-1-78242-223-5.00002-9>.
- AlZohbi, G., Almoaikel, A. & AlShuhail, L. An overview on the technologies used to store hydrogen. *Energy Rep.* **9**, 28–34 (2023).
- Aakko-Saksa, P. T., Cook, C., Kiviahio, J. & Repo, T. Liquid organic hydrogen carriers for transportation and storing of renewable energy – Review and discussion. *J. Power Sources* **396**, 803–823 (2018).
- Singh, R., Singh, M. & Gautam, S. Hydrogen economy, energy, and liquid organic carriers for its mobility. *Mater. Today Proc.* **46**, 5420–5427 (2021).
- Usman, M. R. Hydrogen storage methods: Review and current status. *Renew. Sustain. Energy Rev.* **167**, 112743 (2022).
- Crabtree, R. H. Hydrogen storage in liquid organic heterocycles. *Energy Environ. Sci.* **1**, 134 (2008).
- Müller, K., Völkl, J. & Arlt, W. Thermodynamic evaluation of potential organic hydrogen carriers. *Energy Technol.* **1**, 20–24 (2013).
- Müller, K. et al. Liquid organic hydrogen carriers: thermophysical and thermochemical studies of benzyl- and dibenzyl-toluene derivatives. *Ind. Eng. Chem. Res.* **54**, 7967–7976 (2015).
- Brückner, N. et al. Evaluation of industrially applied heat-transfer fluids as liquid organic hydrogen carrier systems. *ChemSusChem* **7**, 229–235 (2014).
- Okada, Y. Large scale hydrogen energy storage transportation technology “SPERA” system. *Kem. Enjinijaringu* 187–193 (2015).
- Niermann, M., Drünert, S., Kaltschmitt, M. & Bonhoff, K. Liquid organic hydrogen carriers (LOHCs) – techno-economic analysis of LOHCs in a defined process chain. *Energy Environ. Sci.* **12**, 290–307 (2019).
- Scherer, G. Analysis of the seasonal energy storage of hydrogen in liquid organic hydrides. *Int. J. Hydrogen Energy* **23**, 19–25 (1998).
- Teichmann, D. et al. Energy storage in residential and commercial buildings via liquid organic hydrogen carriers (LOHC). *Energy Environ. Sci.* **5**, 9044 (2012).
- Haupt, A. & Müller, K. Integration of a LOHC storage into a heat-controlled CHP system. *Energy* **118**, 1123–1130 (2017).
- Eypasch, M. et al. Model-based techno-economic evaluation of an electricity storage system based on liquid organic hydrogen carriers. *Appl. Energy* **185**, 320–330 (2017).
- Hurskainen, M. & Itonen, J. Techno-economic feasibility of road transport of hydrogen using liquid organic hydrogen carriers. *Int. J. Hydrogen Energy* **45**, 32098–32112 (2020).
- Barhoumi, E. M. et al. Techno-economic analysis of photovoltaic-hydrogen refueling station case study: A transport company Tunis-Tunisia. *Int. J. Hydrogen Energy* **47**, 24523–24532 (2022).
- Ayodele, T. R., Mosetlhe, T. C., Yusuf, A. A. & Ntombela, M. Optimal design of wind-powered hydrogen refuelling station for some selected cities of South Africa. *Int. J. Hydrogen Energy* **46**, 24919–24930 (2021).
- Ampah, J. D. et al. Electric vehicles development in Sub-Saharan Africa: Performance assessment of standalone renewable energy systems for hydrogen refuelling and electricity charging stations (HRECS). *J. Clean. Prod.* **376**, 134238 (2022).
- Chen, Q., Gu, Y., Tang, Z., Wang, D. & Wu, Q. Optimal design and techno-economic assessment of low-carbon hydrogen supply pathways for a refueling station located in Shanghai. *Energy* **237**, 121584 (2021).
- Gökçek, M. & Kale, C. Optimal design of a hydrogen refuelling station (HRFS) powered by hybrid power system. *Energy Convers. Manag.* **161**, 215–224 (2018).
- Siyal, S. H., Mentis, D. & Howells, M. Economic analysis of standalone wind-powered hydrogen refueling stations for road transport at selected sites in Sweden. *Int. J. Hydrogen Energy* **40**, 9855–9865 (2015).
- Zhao, L. & Brouwer, J. Dynamic operation and feasibility study of a self-sustainable hydrogen fueling station using renewable energy sources. *Int. J. Hydrogen Energy* **40**, 3822–3837 (2015).
- Al-Sharafi, A., Sahin, A. Z., Ayar, T. & Yilbas, B. S. Techno-economic analysis and optimization of solar and wind energy systems for power generation and hydrogen production in Saudi Arabia. *Renew. Sustain. Energy Rev.* **69**, 33–49 (2017).
- Gökçek, M. & Kale, C. Techno-economical evaluation of a hydrogen refuelling station powered by Wind-PV hybrid power system: A case study for İzmir-Çeşme. *Int. J. Hydrogen Energy* **43**, 10615–10625 (2018).
- Micena, R. P., Llerena-Pizarro, O. R., de Souza, T. M. & Silveira, J. L. Solar-powered hydrogen refueling stations: a techno-economic analysis. *Int. J. Hydrogen Energy* **45**, 2308–2318 (2020).
- Ulleberg, Ø. & Hancke, R. Techno-economic calculations of small-scale hydrogen supply systems for zero emission transport in Norway. *Int. J. Hydrogen Energy* **45**, 1201–1211 (2020).
- G. Parks, R. B. J. C. and R. R. *Hydrogen Station Compression, Storage, and Dispensing Technical Status and Costs* (2014).
- NREL. System Advisor Model (SAM), SAM2020. <https://sam.nrel.gov/download/version-2021-12-01.html>.
- H2fc, FCEV Sales, FCEB, & Hydrogen Station Data. [https://h2fc.org/by\\_the\\_numbers](https://h2fc.org/by_the_numbers).
- Nel Hydrogen Electrolysers, the world's most efficient and reliable electrolyzers. [www.nelhydrogen.com](http://www.nelhydrogen.com) (2019).

## Acknowledgements

YL and IS acknowledge the funding support from Global Power Generation Australia Pty Ltd and the Australia Research Council in the form of Linkage Project (LP200200472).



### Author contributions

MD: Conceptualization, Methodology, Data curation, Writing- Original draft preparation, Visualization. MW: Visualization, Writing- Reviewing and Editing. AR: Writing- Reviewing and Editing. YL: Supervision, Conceptualization, Reviewing and Editing. IS: Supervision, Conceptualization, Methodology, Reviewing and Editing. KK: Supervision, Conceptualization, Methodology, Reviewing and Editing.

### Declarations

### Competing interests

The authors declare no competing interests.

### Additional information

**Supplementary Information** The online version contains supplementary material available at <https://doi.org/10.1038/s41598-025-91649-x>.

**Correspondence** and requests for materials should be addressed to K.K.

**Reprints and permissions information** is available at [www.nature.com/reprints](http://www.nature.com/reprints).

**Publisher's note** Springer Nature remains neutral with regard to jurisdictional claims in published maps and institutional affiliations.

**Open Access** This article is licensed under a Creative Commons Attribution-NonCommercial-NoDerivatives 4.0 International License, which permits any non-commercial use, sharing, distribution and reproduction in any medium or format, as long as you give appropriate credit to the original author(s) and the source, provide a link to the Creative Commons licence, and indicate if you modified the licensed material. You do not have permission under this licence to share adapted material derived from this article or parts of it. The images or other third party material in this article are included in the article's Creative Commons licence, unless indicated otherwise in a credit line to the material. If material is not included in the article's Creative Commons licence and your intended use is not permitted by statutory regulation or exceeds the permitted use, you will need to obtain permission directly from the copyright holder. To view a copy of this licence, visit <http://creativecommons.org/licenses/by-nc-nd/4.0/>.

© The Author(s) 2025